Conceptual Design And Analysis Of A Supersonic Fighter Aircraft With Low-Boom Technology (SFAwLT)

A project presented to the Faculty of the Department of Aerospace Engineering
San José State University

in partial fulfillment of the requirements for the degree
Master of Science in Aerospace Engineering

by

Zion Amador

June 2022

approved by

Dr. Maria Chierichetti
Faculty Advisor

ABSTRACT

Conceptual Design Of a Supersonic Fighter Aircraft with Low-Boom Technology (Sfawlt)

Zion Amador

The conceptual aircraft design project is an implementation of low boom technology in a fighter aircraft. The design focuses on developing a modern type fighter aircraft using know configurations and techniques to reduce sonic boom production. The design processes conducted for the design follows the classic aircraft design books by J. Roskam and a more modern design procedures from D. Raymer's aircraft design book. The design process covers the sizing, configuration selection, design for the fuselage, wing and empennage. The design processes integrate useful low boom technology and techniques.

ACKNOWLEDGEMENTS

Contents

List of Tables

List of Figures

Abbreviations and Symbols

Abbreviations

AR	Aspect ratio
b	wing span
$\bar{c}$	Mean chord
C_d	Airfoil drag coefficient
C_D	Coefficient of drag
$C_{D,i}$	Induced drag coefficient
C_{Do}	Parasitic drag coefficient
c_f/c	Flap chord ratio
C_l	Airfoil lift coefficient
C_L	Coefficient of lift
C_p	Pressure coefficient
d_f	Fuselage diameter
e	Oswald's efficiency factor
E	Endurance
f	Equivalent parasite area
h	Altitude
H	Height of spike in F-function
L/D	Lift-to-drag ratio
$(L/D)_{max}$	Maximum lift-to-drag ratio
l_f, L	Fuselage length
M	Mach number
MAC	Mean aerodynamic chord
n	Load factor
OEI	One engine inoperative
PLdb	Percieved level in decibel
Ps	Specific excess power
R	Range
RC	Rate of climb
$\bar{q}$	Dynamic pressure
S	Surface area
S_a	Aileron surface area
S_e	Elevator rea
S_{FL}	Landing distance
S_h	Horizontal stabilizer area
S_{TOFL}	Takeoff field length
S_{TOG}	Takeoff ground run
S_v	Vertical stabilizer area
S_{wf}/S	Wing flap area ratio
t/c	Airfoil thickness ratio
T_{req}	Thrust required
TSFC	Thurst specific fuel comsumption
T/W	Thrust-to-weight ratio
$(T/W)_{req}$	Required thrust-to-weight ratio

V	Velocity
V_A	Approach speed
V_{Max}	Maximum velocity
V_{stall}	Stall speed
V_{SL}	Landing stall speed
W_{crew}	Crew weight
W_e/W_0	Empty weight fraction
W_E	Empty weight
W_F	Fuel weight
W/S	Wing loading
W_{tfo}	Trapped (unused) fuel and oil
W_{TO}	Takeoff weight
x_h	Horizontal stabilizer moment arm
x_v	Vertical stabilizer moment arm
Y_f/L	Nose bluntness parameter

Multiple subscripts

$W_{OE,tent}$	Tentative operating weight
$W_{TO,guess}$	Guessed takeoff weight
$W_{E,tent}$	Tentative empty weight
$W_{F,used}$	Used fuel weight
$W_{F,res}$	Fuel reserve weight
S_{wet}/S_{ref}	Wetted area ratio
$C_{L,max}$	Maximum lift coefficient
$C_{L,max,TO}$	Takeoff maximum lift coefficient
$C_{L,max,L}$	Landing maximum lift coefficient
$C_{L,cruise}$	Cruise maximum lift coefficient

Greek

α	Angle of attack
δ_f	Flap deflection
λ	Taper ratio
Λ	Wing sweep
Γ	Dihedral angle
$\dot{\varphi}$	Turn rate
θ_{fc}	Fuselage cone angle

Subscripts

w	Wing
w,LE	Wing, leading edge
w,c/4	Wing quarter chord
w,root	Wing root
w,tip	Wing tip
Δc_l	Lift coefficient increments
$\Delta c_{L,max}$	Maximum lift coefficient incremen

1.0 Introduction

A surge in design and development of supersonic transport (SST) aircraft is seen in today's aerospace industry. New designs push for minimizing the sonic boom phenomenon that occurs when an aircraft surpasses sonic speed. Old and new research for low sonic boom or "low boom" technologies have been tested and proven to minimize the boom effect produced by supersonic aircraft. This project covers the conceptual design process of a fighter aircraft for air superiority. In addition, the aircraft design implements methods, techniques, and technologies to achieve reduction of the sonic boom during its super-cruise segment of flight.

1.1   Literature Review

Literature regarding this topic have been reviewed and will be used as the guidelines for achieving this design. Studies suggests from ballistic wave generated by projectiles moving at supersonic speeds produce sudden overpressures in upstream of the wave and sudden underpressure at the rear part, creating an N-shaped wave of known as "N-wave" pressure signature [1]. Minimization studies have been produced by Buseman [2], Licher [3], NASA, and JAXA and many others show various aircraft designs and configuration for a low-boom aircraft technology.

To properly design a conceptual aircraft with a low boom technology, creating the mission requirements for the aircraft must have appropriate definition. Requirements play a significant role in the entire design process and ultimately the aircraft performance [4]. The mission requirements deriving from the literature available regarding the type of aircraft. Also, customer requirements shape the overall mission requirements of the aircraft [4]. These requirements pose as the problems that require engineers and designers to solve. According to systematic methodology for aircraft concept development [4], problem formulation methods are necessary in aircraft design. The methods include the use of benchmarks, defining the problems, identifying its importance, concept generation, and configuration selection and evaluation [4]. According to various studies [5][6][7][8], Low-Boom supersonic aircraft requirements are as such; cruise velocities of Mach 1.6 – Mach 2.7, altitude of 45,000 ft - 60,000 ft, minimize wing weight, and ground noise level of 70 perceived level in decibel (PLdB). These mission requirements, however, are for supersonic transport aircraft. The geometric requirements are different from the proposal conceptual design of a low-boom supersonic fighter aircraft.

To achieve the requirements set for the aircraft mission requirements, aircraft configuration designs must be in accordance to each requirement. However, during this phase of the design, iterations and tradeoffs are a necessary process in order to acquire the best possible performance for the aircraft. A study illustrates two low-boom and low drag design configurations; the supersonic biplane concept and the supersonic twin-body concept [3]. The biplane concept successfully lowers the shockwave between the biplane wing configuration, providing a 90% wave drag reduction comparison to an equal-volume diamond wedge airfoil [3]. This configuration is an inspiration from studies by Busemann. According to Busemann [2], proper configuration of the aircraft's volume is how one can eliminate the wave drag and sonic boom. The biplane uses two airfoils resulting in a lower wing volume than the conventional diamond wedge airfoil [3]. Moreover, an optimal version of biplane known as the Licher biplane is said to have a larger lift-to-drag ratio (L/D) than the Busemann biplane. The increase in L/D comes from the biplane configuration. The Licher biplane design has a bigger thickness-to-chord ratio for its lower element than the upper element, thus improving the lifting conditions [3]. The next concept introduces the supersonic twin-body configuration. A similar Busemann approach

is taken for this configuration. This concept's configuration has two fuselages, thus the name twin-fuselage. It proposes that over a 20% total drag reduction can be done by an optimal twin-body fuselage in comparison with the Sears–Haack (SH) single-body fuselage, assuming under the constraint of fixed fuselage volume [3].

A more recent concept demonstrator for low-boom supersonic aircraft is the Gulfstream Quiet SpikeTM F-15B. This aircraft test article is a redesign of an F-15B configuration where the nose is able extend upto 30 ft, much like a spike configuration [8]. The theory for this configuration is that the spike would produce weaker shocks or a series of weak shocks; therefore, reducing the initial overpressure and increase the N-wave risetime [8]. The weaker shock generation are due to the aerodynamic shapes placement on the nose of the aircraft. Additionally, a demonstrator under research and development at the Japan Aerospace Exploration Agency (JAXA) known as the Silent Supersonic Technology Demonstrator (S3TD) is a good reference for an intimate configuration [7]. Firstly, the aircraft's airfoil configuration consists of a camber line that is parameterized from a Bezier curve which is linearly interpolated spanwise of the wing. Also, a twist center at 80% of the chord is an implementation for this low-boom purposes. Lastly, the main wing separates into an inboard wing and outboard wing sections [7]. The model from the article shows that the nose of the aircraft has an elongating shape, assuming it would produce the same effect as the Quest Spike by Gulfstream.

Various solutions propose to tackle the low-boom pressure signature. Previous discussions of geometrically shaping the aircraft configuration are design implementations that allow sonic-boom reduction. A more in-depth discussion about these geometrical design strategies is in this section. A study of ballistic waves from projectiles and vehicles of simple geometry provides substantial data about wave profiles. From this study, it examines four types of tests articles are a rifle bullet, the Apollo command module, a rocket shape geometry, and various types of aircraft designs [1]. When a rifle bullet is moving at supersonic speed, it creates a sharp snap sound much like a crack of a whip [1]. The cracking sound is due to overpressure and under pressure of the wave, creating an N wave. In order to calculate the N wave profile, the difference in pressure amplitudes and wave periods are variables to characterize the profile [1]. Moreover, the use of Whitman's function (also called F-function) to calculate the projectiles dimension and shape, is important to calculate the parameters of the N-wave [1]. The next case of the study is the investigation of the sonic boom from the Apollo command module. The study shows interest in the simple and symmetrical shape of the spacecraft. The sonic boom data collections from the spacecraft reentries are records from US Navy ships near the spacecrafts landing trajectories [1]. It should be noted that speeds and altitudes of the space vehicle at some flight points are considerably beyond the technical limits of the military aircraft, therefore Whitham's formalism is useful. Instead, computational fluid dynamic codes like CELHyO-2D and CEDRE determine the space vehicle analysis [1]. Findings from the reentry space craft study concludes three things: laws of fluid dynamics are kept due to the vehicle's diameter at the considered altitudes. Also, under the continuum limit, the round shape detaches the shock from the wall and has a negligeable influence on the pressure profile. More importantly, the near-field pressure signatures of the aerodynamic wake are not N-waves but similar to a blast wave signature [1]. The rocket shape test article uses data from the MIM-23 Hawk surface to air missile for its investigation. Since Whitman's theory of ballistic wave and sonic boom applies preferably to slender and pointed bodies, however, the rocket shape is much more complex than that due to the presence of jets from rockets engines. A computational fluid dynamics model of a rocket shape calculates the sonic boom using parameters from the US standard atmosphere

model and transformation formulas [1]. The use of shape factor equations for the projectile calculation similarly determines the rocket shape's N-wave signature. The results show that among the various sonic boom simulations for a flying rocket, the original model produces the minimum overpressure amplitude [1]. Lastly, a meaningful aircraft examination of numerous experimental test data helps determine sonic boom minimization. The Lockheed F-104 Starfighter which has a simple shape and a close to a body of revolution seems the best design for such an experiment. As comparison for the calculated simulations, flight data from previous flight tests of the F-104 baselines the sonic boom parameters. The collection of data shows that both the original and improved model decrease in overpressure due to increasing the Mach number and the altitude [1]. More importantly, three other models with adjustments according to the aircraft type show conclusions that are identical to those with the blunt and short body configurations from the previous case demonstrators.

A conceptual supersonic aircraft design environment (CSADE) construction bases from the various methods from past studies on sonic boom minimization [9]. This design environment has five components: FGEO, FBOOM, SGD, FWD, and FGA. To generate models, Function of Geometry generate (FGEO) uses a component base approach. Then, Function of sonic boom analysis (FBOOM) analyzes the overpressures using the F function method, and Ray tracing method for ground pressure signatures. In this conceptual design environment, Function of wave drag analysis (FWD) is the wave drag analysis to which uses the supersonic area rule. The analysis determines wave drag coefficients at various roll angles, with sufficient accuracy of no more than 5% error. Lastly, FGA conducts a multi-objective optimization code based on NSGA-II MDO algorithms [9]. Results from the CSADE conceptual design optimized layout has a sonic boom maximum pressure decrease nearly about 17.13%; the maximum pressure is 27.08 Pa and the wave drag coefficient decrease 6.29% [9].

New techniques and practices in flow control studies its effect in sonic boom minimization. Theories suggests flow control can reduce drag and provide shear layer, separation and transition controls [10]. There are different methods to achieve flow control. Strategies notes from different studies use riblets, spanwise blowing pulses of plasma and dynamic roughness [10]. In addition, flow control systems are capable of sufficient control authority during trim and maneuvers without the use of control surfaces [11]. A method of circulation control by the use of a fluid control effector changes aerodynamic forces and moments at fixed angles of attack and fixed geometry, which leads to pressure signature reduction during trim and maneuvers. Another study of flow control uses arc discharge plasma to control oblique shock waves [11]. Investigation has shown that the use of plasma upstream of the oblique shock increases the shock angle. Also, it decreases the Mach number thus statis pressure is increased upstream and decreased behind the shock.

According to Seebass and George [2], undesirable features of the overpressure signature require special aerodynamic designs. Aircraft shaping can provide the desire of pressure variations between shockwaves. A discussion of minimizing pressure must meet certain conditions [10]. To minimize the pressures in the sonic-boom signature, diminishing the F subject to the constraint for sonic-boom minimization is key. Secondly, the lines with slope constant B should provide a bow shock with strength proportional to constant A. The third condition is the prescription of the ratio of the front and rear shock strengths. Finally, the area under the F curve must be equal to that under the slope the constant B. Results from this experiment suggests that improvements in shock pressure rise and overpressure require an increase in the impulse. If the decision is to eliminate the shock waves entirely, then there must

be no discontinuity. More importantly, supersonic transports with acceptable sonic-boom overpressure signatures may be possible. Overpressure reductions and shock pressure rise, impulse annoyance, damage and avalanche still require further investigation [2].

Further study claims that nose-bluntness relaxation may reduce sonic-boom for supersonic cruise conditions. The paper describes F-function represents a distribution of sources which causes the same disturbances as the aircraft at some distance from the aircraft [6]. In all instances observe that overpressure levels decrease with length. Though these results are for minimum-overpressure signatures, similar trends are found to exist for the minimum-shock signatures [6].

Different methods are available for testing new conceptual designs for low-boom supersonic aircraft. Models undergo optimization and simulations using numerical analysis and computational fluid dynamics (CFD). Numerical simulation methods simulate a diffracted U-shaped sonic boom waveform [12]. Methods of numerical simulations developments are for specific reasons. Using the nonlinear Tricomo equation (NTE) simulates the focus boom or the carpet boom. In addition, to simulate the signature of the sonic boom, the Burges equation is known to work best. Lastly, the literature [12] explains the use of the Khokhlov-Zabolotskaya-Kuznetsov (KZK) method. It is useful for solving atmospheric turbulence effects towards sonic boom signatures of a supersonic aircraft. Results from these methods of predicting U-shaped sonic boom are comparable to the predicted signatures from the D-SEND #2 flight test, therefore, proving its validation. The predicted result shows reasonable agreement with the measured signatures except for the amplitude in the tail shock wave. An assumption for the discrepancy leans towards the effects of atmospheric turbulence [12][13]. A quick observation notes that the low-boom waveform considered in this paper is more likely to have much gentler wavefront than a conventional N wave. Though many sharp peaks or rounded waveforms, SPnoise simulation of sonic boom successfully simulates rounded waveform very similar to that obtained from the flight test [13].

Predictions of sonic boom are known to use computational fluid dynamics (CFD) methods. Early methods and theories such as the Busemann, Seebass, Darden, and etc. developments investigate sonic boom minimization. This study explores the parameters that affects the sonic boom signature. The simulations examine parametric variables of flight altitude, Mach number, con half-angle, bluntness and fineness ratio [14]. Simulation of the cone half-angle parameter findings suggests that angles between 6.46 deg to 12.75 deg of cone half-angle show only 0.09 psf increase [14]. When it comes to the effect of the bluntness of the aircraft, optimal measurement determination selections cover various speeds. The speeds under inquiry are Mach 1.4, Mach 2.01, Mach 2.96, Mach 3.83, Mach 4.63 [14]. The respective radii for each speed are 0.62 for Mach 1.4, 0.49 for Mach 2.01, 0.4 for Mach 2.96, 0.36 for 3.83, and 0.38 for Mach 4.63 [14]. These results show a pattern for overpressures produced, which entail those faster speeds are optimal with smaller bluntness radius. In contrast, impulse production by different bluntness shape shows that, higher ratios are optimal for minimizing impulse. The next parameter investigates the fineness ratio of the nose to body of the aircraft. The test model designs are to be under the condition of the same bluntness parameter. Results show that the fineness ratio effect are linearly increasing the overpressures and impulse. Findings show that these growth rate of the overpressures and impulse slightly decrease with increasing speeds [14]. Lastly, investigation of how the effects of Mach number and altitude play their roles in minimizing overpressures and impulse. The experiments support that flight altitude does reduce sonic boom effects. More importantly, the study expresses that overpressure increase along with

increase in Mach number [14]. Impulse results show similar trends with overpressures results. In all, these parameters may play significance in designing low-boom aircraft technologies. Each parameter are products that can result in optimal minimization in both overpressures and impulse.

This is a study on integrating low-fidelity MDO and CFD based redesign of a low-boom supersonic aircraft. The study provides information on how CFD plays a significant role in aircraft design optimization. The block coordinate optimization (BCO) method expands to find an approximate solution of the mixed-fidelity low-boom MDO problem [15]. This is a method of finding optimal combination of cruise speed, cruise altitude, range, and weight for a CFD-based low-boom design. Two significant optimization methods improve the design successfully. First, a system-level trade method is to find the highest cruise speed and longest range for a specific cruise altitude [15]. Also, the integration demonstrates the potential sonic boom noise level under 70 perceived level in decibel (PLdB) on the ground [15]. According to the optimization results [15], the speed shows an increase from Mach 1.6 to Mach 1.8. Additionally, the maximum range also lengthen from 2500 nm to 2950 nm. This study is able to show that system-level trades among the target PLdB, cruise Mach, cruise altitude, and range are critical for development of economically viable low-boom supersonic transports. More importantly, minor wing modifications of a low-boom low-weight design from low-fidelity MDO can result in a CFD-based low-boom design with a reversed equivalent area close to a low-boom target below 70 PLdB [15].

Lastly, a faster simulation within a stratified atmosphere, extending from a supersonic flying body down to the ground has been successfully achieved by means of a space marching method with semi-adapted structured grids [16]. Discussions in workshops express those primary sonic booms at cruise are accurately predictable by the use near-field CFD analysis and viscous effects at high Re and the Burgers equation. The methodology for to this CFD analysis is the space marching method. This method reduces computational cost [16]. More importantly, the CFD analysis compares to the D-SEND#1 drop test for accuracy. The results show that the grid resolution to evaluate sonic boom propagation simulation in the near-field using the space marching method have comparable levels of accuracy. This study concludes that far-field waveforms are comparable to results from previous studies. Also, note that the computational cost in a space marching method is less than 1% of the cost requirement for a time marching method [16].

1.2   Motivation

The motivation of this project is to integrate the technologies from these studies in an air-superiority fighter aircraft. There has been no known focus in fighter aircraft designs that implement low-boom technologies. Therefore, this project focuses on achieving characteristics of an air-superiority fighter aircraft while implementing the design features of low-boom technologies to achieve a reduction in sonic boom pressure signatures in both near field and ground level. To verify the design's pressure signatures, computational fluid dynamic (CFD) analysis will be done on the completed conceptual design. Properties under focus will be the N-wave pressure signatures on near field and ground levels as well as noise levels. Results will be compared to completed studies from the reviewed literature.

1.3 Comparative Studies of Similar Aircraft

1.3.1 Introduction

Military fighter aircraft are one of the most complex technologies in aviation. They serve many purpose in military strategy. Controlling the airspace produce safety and security. Air-superiority aircraft serves such purpose. They control the airspace with ease through rapid interception, air-to-air combat, and ground support. Listed below are great examples of air-superiority aircraft.

Ten aircraft were reviewed for the similar aircraft study. Out of the ten, five aircraft were considered for this design. The five aircraft are: Sukhoi SU-15 "Flagon", F-14 "Tomcat", F-15 "Eagle", MIG-29 "Fulcrum", and MIG-31 "Foxhound". The SU-15 is a long-range interceptor that was developed by the Soviet Union in 1965. Similarities that were investigated were its payload, armaments, and dimensions. The F-14 was a well-known air-superiority aircraft which had multi-roles such as interceptor, air-to-air fighter, and aerial reconnaissance. Initial interest was its variable sweep wings, mainplane structure, and dimensions. The F-15's range capabilities, maximum velocity and configurations were great characteristics to implement in this design. Lastly, the MIGs service ceiling, air-to-air combat capabilities, maximum speed and armament were considered for the design.

1.3.2 Configurations and Roles

These aircraft were built for specific missions and roles in the air. To be successful in its missions, each aircraft had to be configured to meet the necessary requirements placed by the designers. The configurations covered in the table below were the wing planform, propulsion, empennage, crew, and landing gear. Most of the aircraft considered had similar configurations. Moreover, the similar aircraft study investigated the roles of each aircraft. All but one, SU-15, were all air superiority aircraft. Their main purpose was to rule the airspace with air-to-air combat capabilities, interception, and ground support/attack.

Table 1 Comparable aircraft configurations and capabilities [17][18][19][20][21][22][23]

Name	Image	Configuration	Roles
SU-15 (1965)		• Trapezoidal wing • 2 Turbojet engine • Conventional empennage • 1 crew • Tricycle landing gear	• Interceptor
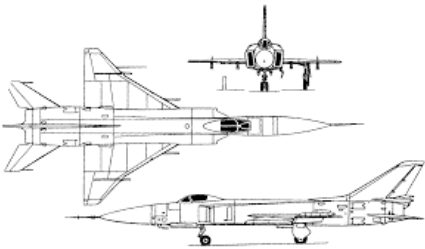
F-14 (1970)	• Variable sweep wing • 2 Turbofan engine • Conventional empennage • 2 crew • Tricycle landing gear	• Air superiority • Interceptor • Aerial reconnaissance • Multirole
F-15 (1976)	• Swept wing • 2 Turbofan engine • Conventional empennage • 1 crew • Tricycle landing gear	• Air superiority • Dual role
MIG-29 (1977)	• Swept wing • 2 Turbofan engine • Conventional empennage • 1 crew • Tricycle landing gear	• Air superiority • Multirole
MIG-31 (1979)	• Swept wing • 2 Turbofan engine • Conventional empennage • 2 crew • Tricycle landing gear	• Interceptor
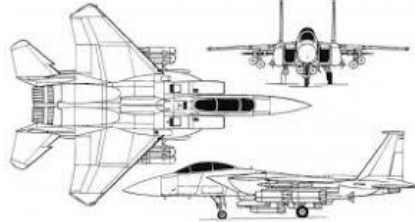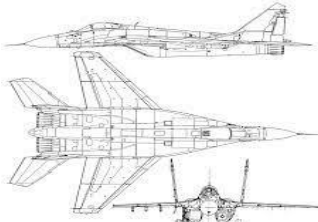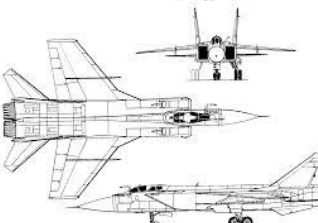
1.3.3 Comparison of Design Parameters

In this similar aircraft study, it was important to review each aircraft's design parameters such as its wing loading, thrust-to-weight ratio, and weight. These parameters greatly affect the design of the aircraft. More importantly, these parameters were useful guidelines and baselines for the sizing and design of the aircraft.

Table 2 Aircraft Parameters Comparison [17][18][19][20][21][22][23]

Parameter	Units	SU-15	F-14	F-15	MIG 29	MIG-31
W_{TO}	lb	37,920	70,345	44,500	37,037	80,953
W_E	lb	23,973	39,930	28,700	24,030	48,100
W_F	lb	12,345	24,912	36,200	8,818	31,305
W/S_g	lb/ft²	96	124.5	73.2	90.5	122.5
Thrust (dry)/ (afterburner)	lbf	18,682	25,000	17,800/ 29,100	22,302	41,814
T/W_g	--	.49	.57	1.07	1.09	.85
TSFC (dry/ (afterburner)	lb/h*lb f)	.93/2.09	.88/2.26	.76/1.94	.77/2.05	.72/1.86
Range	nmi	961	1,620.8	2,088.7	802.6	1,620.8
V_{Max}	mph	1,386	1,584	1,676	1,532	1,864

Climb rate	ft/min	45,000	45,000	50,000	65,000	41,000
Ceiling	ft	60,000	50,000	65,000	59,000	67,651
S	ft^2	394	565	608	409	663
b	ft	30.7	64.1/37.6	42.8	37.3	44
AR	--	--	7.3/2.5	3.01	3.4	2.94
Length	ft	67.42	62.7	63.8	56.8	74.2
Payload	lb	3,086	5,687	4,800	10,582	22,429

1.3.4 Discussion and Conclusion

All five aircraft considered for the similar aircraft study had different parameters. Three out of the five aircraft only required one crew to operate the aircraft. However, this configuration was not able to impact the length of the aircraft since most were around the same lengths. The aircraft propulsion configurations seemed to lean more with two engines, where most of the engines were turbofan with afterburners. It was observed the aspect ratios of the aircraft were between 2.5 – 3.4.

Also, comparing the performance parameters, the almost all had incredibly fast rates of climb which were above 50,000 ft/min. However, the biggest difference amongst the five were the payload capabilities. The Russian aircraft seemed to have the greatest payload of more than 10,000 lbs. The MIG-29 was the lighter aircraft of the two, however, it still managed to carry such heavy payload. Lastly, the wing loading found in the five aircraft were seen to be dispersed. The F-15 had the lowest wing loading; however, the MIG-31 had the largest wing area. The lower wing loading seemed to have provided benefits for the aircraft's performance, such as range, service ceiling, and weight.

It was concluded that for the design, the best aircraft considered for similarities in the design was the F-15. The F-15 was the lighter aircraft with the highest maximum velocity. Furthermore, its range capability was the number one out of the five. However, the F-15 did not have adequate payload capacity. Other aircraft were considered to produce a higher payload capacity, such as the MIG-29. These two aircraft were studied to be the best fit for guiding the conceptual design for this project.

2.0 Mission Specification

2.1 Mission Description

The mission for the aircraft is based on the five similar aircraft capabilities. It must be noted that only three of the five similar aircraft are still in service. These aircraft are the 4th generation fighters, which still have the abilities and capabilities to fly against today's fighters such as the F-22, F-35, SU-57, and J-20 aircraft.

Table 3 Mission specifications and requirements [5][6][7][8]

Payload:	20 mm automatic cannons with 1,000 lbs of ammunition (the cannon weight of 250 lb is part of W_E). Internally carried four 80 lb short, four 500 lb medium and two 1,000 lb long range air-to-air missiles. Weapon drops are mission dependent.
Crew:	One pilot (250 lb max)
Range and Altitude:	See mission profile. No reserves.
Cruise Speed	500 kts at 15,000 ft, clean. M = 2.2 at 50,000 ft, clean. M = 1.4 at 47,000 ft, clean.
Climb	Direct climb to 45,000 ft at max W_{TO} in 6 minutes is desired under subsonic speed. Climb gradient must be more than 250 ft/nmi. Supersonic climb from 45,000 ft to 50,000 ft. Climb rate on one engine at max W_{TO} must be greater than 500 ft/min.
Take-off and Landing:	Ground run of less than 2,500 ft at sea level. Field length no greater than 3,000 ft for take-off and 5,000 ft for landing. All at sea level
Service Ceiling:	50,000 ft. Combat ceiling: subsonic max power = 500 ft/min. supersonic max power = 1,000 ft/min. Cruise ceiling: subsonic max continuous power = 300 ft/min. supersonic continuous power = 1,000 ft/min.
Maneuverability	Turn rate must be greater than 12° per second with less than 4,500 ft turn radius at an altitude of 15,000 ft. Load factor of 7 Gs with velocity of 590 kts at an altitude of 15,000 ft.
Certification Base:	Military
Low Boom	Noise signatures PLdB must be less than 70 dB.

2.2 Mission Profile

The aircraft's mission profile was the flight pattern that must be followed for a specific mission. These mission profiles consisted of various segments of the aircraft's capabilities for the mission to be considered successful. There were 14 total segments for the aircraft's mission profile. Below was created to show the mission profile which includes the altitudes and ranges for each mission.
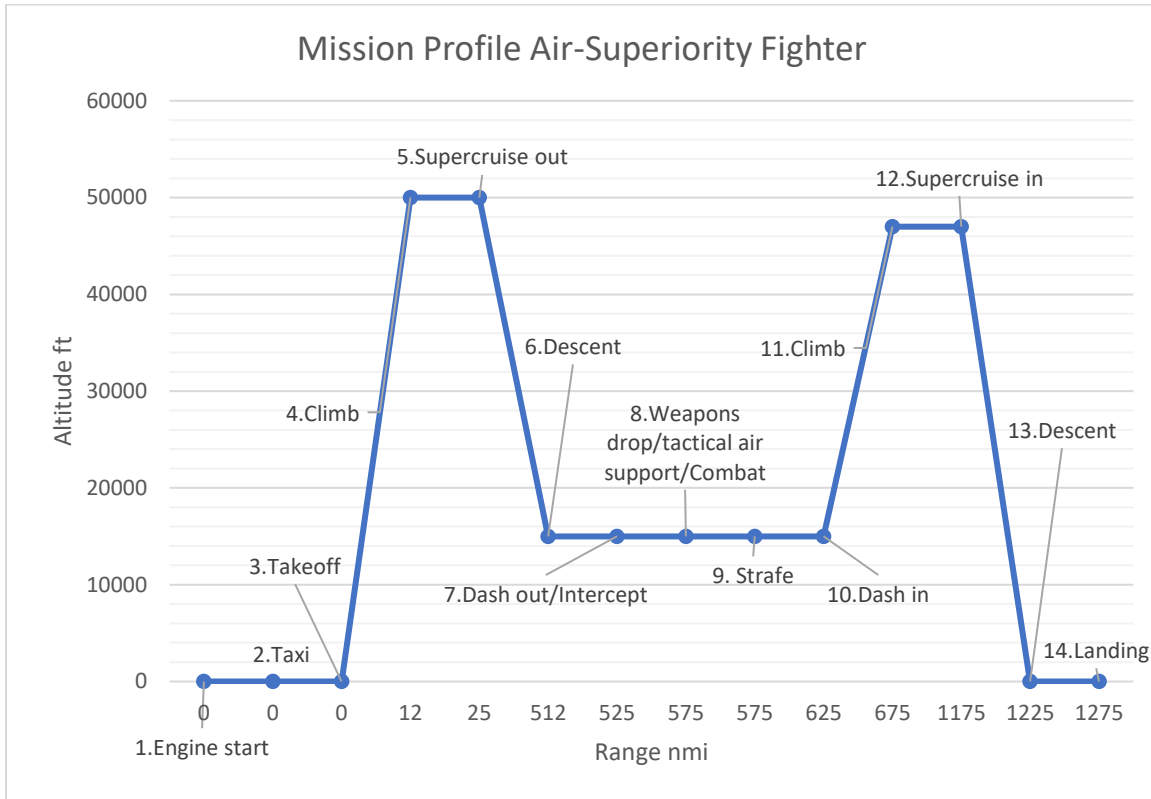
Figure 1 Mission profile for air-superiority fighter aircraft

2.3 Critical Mission Requirements

As stated in the introduction, this aircraft design is for air-superiority, however, it is a major requirement to which sonic boom minimizations with the use of low boom technologies must be met. Moreover, the aircraft design must have air-superiority fighter capabilities such as air-to-air combat, interception, and ground support to ensure the safety of airspace over land or sea. The success of the design allows supersonic fighter aircraft to be flown at supersonic speeds over any terrain without environmental and physical consequences to the surroundings below.

2.4 Measures of Merit

1. A fighter aircraft which is capable of supersonic flight over land with a reduced sonic boom noise propagation less than 70 PLdB.

2. Lengthy range performance can extend mission capabilities which can add mission success for providing larger area coverage of air space support and safety.

3. Cost effective when it comes to jet fuel usage, since the design allows optimal range with minimum fuel consumption.

2.5   Discussion

Mission specifications and requirements produced for the aircraft's design were workable for any fighter aircraft. The payload capacity required were not far from the similar aircraft study. The requirements were enough for the aircraft to perform air-to-air combat missions with its armaments, but also able to accomplish weapons drop missions, or ground support mission.

In the design the list requirements noted the various cruise velocities in the aircraft's mission profile. The aircraft was required to perform two supercruise flight segments (intercept) and two low altitude subsonic cruise (dash). These velocity requirements were related to the aircraft's noise profile during supercruise. The aircraft's supercruise segments had to achieve the low boom requirements since these missions were mostly meant to be over land terrains. Moreover, the aircraft was required to perform two different supercruise speeds at two different altitudes. This requirement had to do with the second climb segment. In order to achieve the second climb segment, a combination of climb and acceleration to a higher altitude and supersonic end velocity was considered. Therefore, it was noted that a lowered supercruise altitude for this segment would consume less fuel.

Lastly, the mission profile showed in detail each phase of the mission. For an air-superiority aircraft, these various phases must be within its capabilities. It provided a good visualization of the aircraft's speed, altitudes, range and even various types of combat missions.

3.0 Sizing

3.1 Weight Sizing

Once the requirements were formed, the next step was to determine the sizing parameters for the aircraft. The aircraft's initial weight estimates were both calculated by hand using the step-by-step process from Roskam's methods [24], and by Raymer Design Software (RDS) "Quick Initial Sizing tool" [25].

3.2 Mission Weight Estimates
3.2.1 Manual Weight Estimation (Roskam's Method) [24]

Implantation of Roskam's methods for weight estimates using Matlab calculated the initial weight approximation of the takeoff weight (W_{TO}), empty weight (W_E), fuel weight (W_F) were all calculated. The fuel fraction method was used to determine these aircraft weight estimates for the initial weight sizing. The steps included:

Step 1. Determined the mission payload weight, (W_{PL})
Step 2. Provided a guessed value for the takeoff weight ($W_{TO,guess}$)
Step 3. Determined the mission fuel weight, (W_F)
Step 4. Calculated a tentative operating empty weight value ($W_{OE,tent}$)

$$W_{OE,tent} = W_{TO,guess} - W_F - W_{PL} \tag{3.1}$$

Step 5. Calculated a tentative empty weight value ($W_{E,tent}$)

$$W_{E,tent} = W_{OE,tent} - W_{tfo} - W_{crew} \tag{3.2}$$

where the trapped (unusable) fuel and oil (W_{tfo}) amount was considered as .5% of the W_{TO}.
Step 6. Found the allowable value of W_E
Step 7. Compared the values for $W_{E,tent}$ and for W_E. (Reiterated steps until $W_{E,tent}$ and W_E agreed with each other within the pre-selected tolerance of 0.5%.

3.2.1.1 Determine the Mission Payload

Payload weight (W_{PL}) determination was specified in the mission requirements. For this specific aircraft, the payload weight were all military loads such as ammunition, bombs, and missiles. A maximum payload of 6,000 lb was determined for the aircraft's initial weight estimation. The 6,000 lb payload weight includes combat segment and weapons drop segment. Due to estimation purposes, the four medium range air-to-air missiles was not included in the payload weight to accommodate for the weapons drop payload.

Table 4 Weight breakdown of aircraft payloads

Payload	Count	Weight (lb)
20 mm Cannon Ammunition	--	1,000
Short Range Air-to-Air Missiles	4	80

Medium Range Air-to-Air Missiles (not included in weight estimation)	4	500
Long Range Air-to-Air Missiles	2	1,000
Weapons drop (bombs)	--	2,000
Total		**7,320**

3.2.1.2 Provide a Guessed Value

In order to provide an accurate guessed takeoff weight ($W_{TO,guess}$), the similar aircrafts takeoff weight data was used as comparisons. The various takeoff weights for the similar aircrafts were between 35,000 lb and 90,000 lb. The averaged weight of the five similar aircrafts was a little over 54,000 lb. It was believed that using a higher guess takeoff weight value, $W_{TO,guess} = 60,000$ lb, would help decrease the needed iterations to determine the actual calculated takeoff weight.

3.2.1.3 Determine Fuel Weight Using Mission-Segment Weight Fractions

This section used a method called fuel fractioning and obtain a calculated fuel weight for this design. The calculated fuel weight (W_F) included fuel the aircraft used during the entirety of its mission and its fuel reserves.

To determine the mission fuel weight, fuel used at each mission segment was determined using data provided by Roskam [24]. Additionally, segments such as cruise, weapons drop, and strafe used provided equations to calculate their fuel fractions.

$$W_F = W_{F,used} + W_{F,res} \tag{3.3}$$

where: $W_{F,used}$ is fuel used during the mission
$W_{F,res}$ are the fuel reserves required for the mission

Important data used for the fuel fraction calculation provided by Roskam [24]. The supersonic cruise airplane type data was used for these segments:

- Engine Start, Warm-up: 0.990
- Taxi: 0.995
- Takeoff: 0.995
- Climb: 0.92 - 0.87
- Descent: 0.985
- Landing, Taxi, Shutdown: 0.992

Calculated values for the cruise segments and strafe were determined using the Breguet's equations for range and endurance for jet engine aircraft [24].

$$R = (V/c_j) \times (L/D) \times \ln(W_i/W_{i+1}) \tag{3.4}$$

$$E = (1/c_j) \times (L/D) \times \ln(W_i/W_{i+1}) \tag{3.5}$$

Where for supersonic cruise aircraft:
- Cruise Segment
  - Lift-to-Drag Ratio (L/D) = 4 − 6

- o Specific fuel consumption for jet engines (c_j) = 0.5 – 0.9 lbs/lbs/hr
- Strafe (Endurance) Segment
  - o L/D = 7 – 9
  - o c_j = 0.6 – 0.8

Table 5 Fuel-fraction calculation using Roskam's method [24]

1.	**Warm up**	$W_1/W_0 = 0.990$
2.	**Taxi**	$W_1/W_2 = 0.990$
3.	**Take off**	$W_3/W_2 = 0.990$
4.	**Climb**	$W_3/W_4 = 0.88$
5.	**Supercruise**	R = 500 nmi = 3.0381E+6 ft
		c_j = 0.8 1/hr = 0.000222 1/s
		V = 2.2 Mach x (994.8 ft/s) = 2,188 ft/s
		L/D = 6
		$W_5/W_4 = e^{(-R*c_j/V*L/D)}$
		= 0.95
6.	**Descend**	$W_6/W_5 = 0.985$
7.	**Cruise (dash)**	R = 50 nmi = 303,806 ft
		c_j = 0.8 1/hr = 0.000222 1/s
		V = .8 Mach x (994.8 ft/s) = 795.8 ft/s
		L/D = 6
		$W_7/W_6 = e^{(-R*c_j/V*L/D)}$
		= 0.986
8.	**Weapons drop/Combat**	$W_8/W_7 = 1$
		Subtract payload drop from current total fuel fraction:
		$(W_{TO,guess} * (1 - M_{ff(1-7)})) –$ Weapons drop weight (W_{PL})
9.	**Strafe**	E = 5 min = 300 s
		c_j = 0.8 1/hr = 0.000222 1/s
		L/D = 6
		$W_9/W_8 = e^{(-E*c_j/(L/D))}$
		Corrected $W_9/W_8 = (1 – (1 – W_9/W_8) * W_8/W_7)$
		= 0.996
		$W_9/W_{8,ammo\ burst} = 0.9928$
10.	**Cruise (dash)**	R = 50 nmi = 303,806 ft
		c_j = 0.8 1/hr = 0.000222 1/s
		V = .8 Mach x (994.8 ft/s) = 795.8 ft/s
		L/D = 6
		$W_{10}/W_9 = e^{(-R*c_j/V*L/D)}$
		Corrected $W_{10}/W_9 = (1 – (1 – W_{10}/W_9) * W_9/W_{8,ammo\ burst})$
		= 0.986
11.	**Climb**	$W_{11}/W_{10} = 0.90$
12.	**Supercruise**	R = 500 nmi = 3.0381E+6 ft
		c_j = 0.8 1/hr = 0.000194 1/s
		V = 1.4 Mach x (994.8 ft/s) = 1,392.7 ft/s
		L/D = 6
		$W_{12}/W_{11} = e^{(-R*c_j/V*L/D)}$
		= 0.922
13.	**Descend**	W_{13}/W_{12} = .990
14.	**Landing**	W_{14}/W_{13} = .985

$$\mathbf{M_{ff}} = \frac{W_{14}}{W_{13}} \frac{W_{13}}{W_{12}} \frac{W_{12}}{W_{11}} \ldots \ldots \frac{W_4}{W_3} \frac{W_3}{W_2} \frac{W_2}{W_1} \frac{W_1}{W_0}$$

= (0.990) · (0.990) · (0.990) · (0.88) · (0.95) · (0.985) · (0.986) · (1) · (0.996) · (0.986) · (0.90) · (0.922) · (0.990) · (0.985)

$$\mathbf{M_{ff}} = 0.626$$

$\mathbf{W_F} = M_{ff} \times W_{TO,guess}$;
where: $W_{TO,guess}$ = 60,000 lb and W_{PL} = 6,000 lb
$$\mathbf{W_F} = 22,437 \text{ lb}$$

3.2.1.4 Determine the Empty Weight

Following steps 4 and 5, the empty weight estimation W_E were solved with the initial takeoff guess weight ($W_{TO,guess}$) = 60,000 lb and payload weight (W_{PL}) = 6,000 lb.

$$W_{OE,tent} = W_{TO,guess} - W_F - W_{PL}$$
$$= 60,000 - 22,560 - 6,000$$
$$= 31,440 \text{ lb}$$

$$W_E = W_{OE,tent} - W_{tfo} - W_{crew}$$
$$= 31,440 - (60,000 \times 0.005) - 250$$
$$= 30,890 \text{ lb}$$

$$\frac{|W_{OE,tent} - W_E|}{[\frac{(W_{OE,tent} + W_E)}{2}]} \times 100 < 0.5\%$$

$$\frac{|31,440 - 30,890|}{[\frac{(31,440 + 30,890)}{2}]} \times 100 = 1.76\%$$

The initial guess takeoff weight ($W_{TO,guess}$) estimate of 60,000 lb, the difference between the tentative empty weight ($W_{OE,tent}$) and the calculated empty weight (W_E) was higher than .5%. Therefore, more iterations of guesses were conducted until the 0.5% difference was satisfied.

3.2.1.5 Determine Take-off Weight

The take-off weight (W_{TO}) was determined once a tolerance of less than 0.5% between the operational tentative empty weight ($W_{E,tent}$) and the calculated empty weight (W_E). Since the aircraft was required to fly at supersonic cruise, a weight trend for supersonic cruise airplanes was used to determine the gross take-off weight in relation to the accepted empty weight.

After the first iteration of weight estimates. The gross take-off weight, empty weight, and fuel weight were determined using the weight trends provided from Roskam's Preliminary Sizing book. The first iteration did not meet the percent difference between the guessed take-off weight and the calculated take-off gross weight of 2%. The table below were the results of four iteration.

$$W_F = 22,560 \text{ lb}$$
$$W_E = 30,890 \text{ lb}$$
$$W_{TO,guess} = 60,000 \text{ lb}$$
$$W_{TOG} = 68,000 \text{ lb}$$

$$|W_{TO,guess} - W_{TOG}| \div [\frac{(W_{TO,guess} + W_{TOG})}{2}] \times 100 < .2\%$$

$$|60,000 - 65,000| \div [\frac{60,000 + 72,000}{2}] \times 100 = 12.5\%$$

15

Table 6 Takeoff weight W_{TO} calculation iterations values

Iteration #	$W_{TO,guess}$	W_F	W_E	$W_{TO,calculated}$
1	60,000	22,560	30,890	68,000
2	50,000	18,800	24,700	56,500
3	47,000	17,672	22,843	51,200
4	45,000	16,920	21,605	49,000
5	40,000	15,040	18,510	42,000
6	38,000	14,288	17,272	38,450
7	35,000	13,160	15,415	35,000

After seven iterations, it was calculated that the initial takeoff weight (W_{TO}) for the aircraft was 35,000 lb. Although, the calculated weight difference between the tentative operational empty weight and calculated tentative weight was above the 0.5% suggested value, the guess weight ($W_{TO,guess}$) and calculated weight (W_{TO}) difference were under the 0.2% mark. Figure 2 was used to determine the calculated takeoff weight. The figure provided a trendline for supersonic cruise aircraft takeoff weight (W_{TO}) estimation in relation to the calculated empty weight (W_E). In this figure, the red markings showed the intersected point for the estimated takeoff weight (W_{TO}) and the calculated empty weight (W_E)
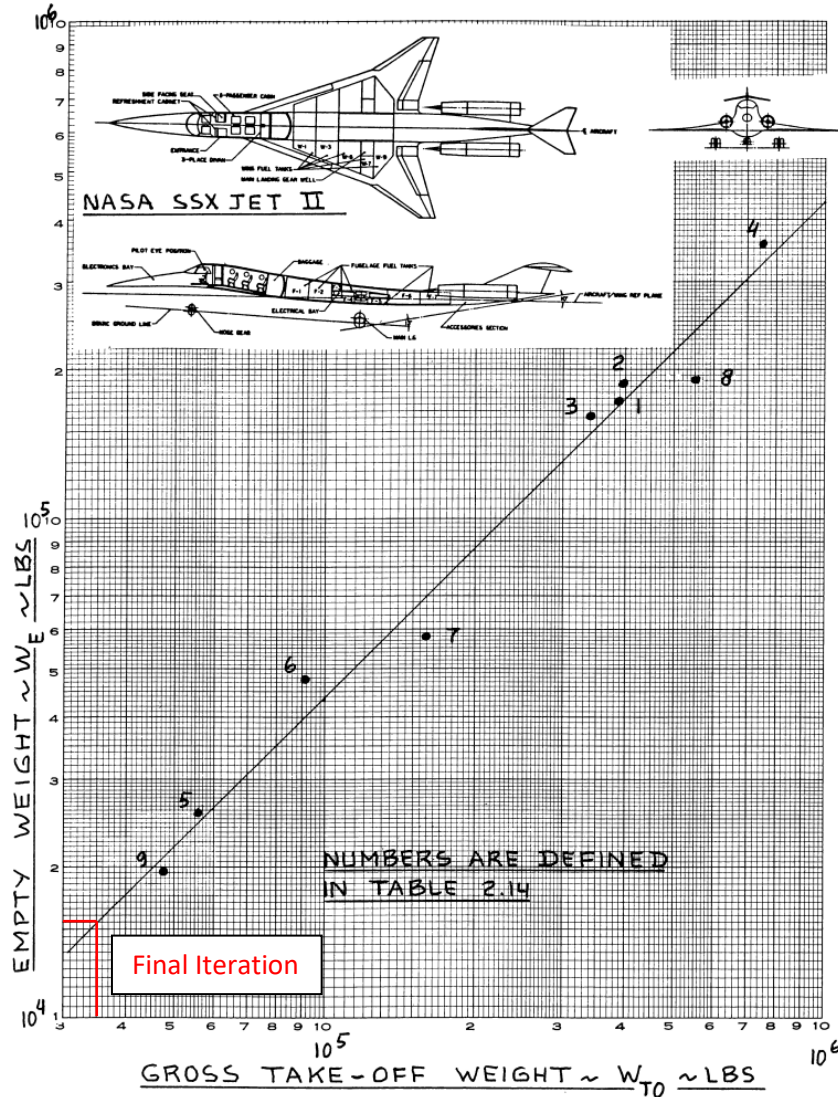
Figure 2 Roskam's weight trends for supersonic cruise aircraft

3.2.2 Raymer's Aircraft Design Software "RDS" Weight Estimation

Daniel Raymer is well known for his aircraft design books much like Roskam. He uses more modern methods for aircraft design. Using the advancement in technology, Raymer develops his own aircraft design software called RDS which implements his aircraft design methods. This section uses that tool to determine a weight estimation for the air-superiority aircraft design [25].

3.2.2.1 RDS Quick Initial Sizing Tool

The RDS used Raymer's method of weight estimation. This method was known to produce more accurate empty weight estimation. It required more complex inputs than Roskam's method.

Like the Roskam's method of calculating for the initial weight of the aircraft, a guess takeoff weight ($W_{TO,guess}$) of 60,000 lb was entered. Also, the same values of crew and payload weight were used. To determine the wing area ratio (S_{wet}/S_{ref}), Raymer provided historical data

17

gathered for various aircraft configuration [9]. It was assumed that the aircraft would have a low wing area, therefore, the value of 4.2 was preferred. Moreover, the selected aspect ratio was purely based from the similar aircraft data average of about 3.

Table 7 RDS quick initial sizing tool user input for aircraft properties [25]

Step 1	Enter guess takeoff weight:	60,000 lb
Step 2	Enter the crew, cargo, and passenger weight:	250 lb | 6000 lb | 0 lb
Step 3	Select aircraft category to estimate empty weight fraction (W_e/W_0):	Jet fighter
Step 4	Enter the fudge factor (default = 1):	1
Step 5	Select category of aircraft to estimate the equivalent skin friction coefficient:	Navy fighter
Step 6	Enter the ratio of wetted area to the wing reference area (S_{wet}/S_{ref}):	4.2
Step 7	Enter Parasitic fudge factor (default = 1):	1
Step 8	Enter the estimated Aspect Ratio (AR):	3
Step 9	Estimate the Oswald Efficiency Factor (e):	0.35
Step 10	Enter wing loading W/S:	131 lb/sqft
Step 11	Enter propulsion type:	Jet propulsion
Step 12	Enter engine thrust-to-weight ratio (T/W):	0.51
Step13	Enter engine thrust specific fuel consumption (TSFC):	1.94 (after burning engine)
Step 14:	Enter number of engines:	2
Step 15:	Enter desired range:	1,200 nmi

3.2.3 RDS Mission Sizing and Range Results

After all data needed was entered in the Quick Initial sizing tool, the software has a Sizing and Range analysis tool. The figures shown below are the many mission segments for the aircraft. The analysis tool allowed specific input values such as altitude, velocity, range, thrust setting and more. There were 13 total segments that were analyzed. Table 8 and 9 included; takeoff, climb to 45,000 feet with end velocity of Mach .85, accelerated to Mach 1.7 while climbing to cruise altitude of 50,000 feet, and accelerated to Mach 2.1 for the cruise segment. The weight drop segment, combat, dash in, and climb back to cruise altitude were covered in Table 10. Finally, Table 11 completed the mission with supercruise in segment at Mach 1.4 followed by decent and landing.

Table 8 RDS weight and range sizing segments 1-4

MISSION SIZING OR RANGE: AdvFtr_SFAwLT.dms.rdsdms

FPS		Enter analysis input parameters. For help click on column titles.					
1 TAKEOFF		2 CLIMB/ACCEL		3 CLIMB/ACCEL		4 CLIMB/ACCEL	
THRUST SETTING	Max	THRUST SETTING	100.	THRUST SETTING	100.	THRUST SETTING	Part AB
ALTITUDE	0.0	STARTING ALT	0.0	STARTING ALT	45000.	STARTING ALT	50000.
TIME	0.0083	END ALT	45000.	END ALT	50000.	END ALT	50000.
(n/a)	0.0	START VEL	0.4	START VEL	0.85	START VEL	1.7
(n/a)	0.0	END VEL	0.85	END VEL	1.7	END VEL	2.1
(n/a)	0.0	AlternatePolar#	0.0	AlternatePolar#	0.0	AlternatePolar#	0.0

Table 9 RDS weight and range sizing segments 4-7

MISSION SIZING OR RANGE: AdvFtr_SFAwLT.dms.rdsdms

FPS		Enter analysis input parameters. For help click on column titles.					
4 CLIMB/ACCEL		5 CRUISE		6 CRUISE		7 WEIGHT DROP & TURNAROUND	
THRUST SETTING	Part AB	THRUST SETTING	Part AB	THRUST SETTING	100.	(n/a)	0.0
STARTING ALT	50000.	ALTITUDE	50000.	ALTITUDE	15000.	Weight DROPPED	5000.
END ALT	50000.	VELOCITY	2.1	VELOCITY	500.	(n/a)	0.0
START VEL	1.7	RANGE	500.	RANGE	50.	#DropExt.Stores	0.0
END VEL	2.1	Find Range	No	Find Range	No	Turnaround	Yes
AlternatePolar#	0.0	AlternatePolar#	0.0	AlternatePolar#	0.0	BeginReserve	No

Table 10 RDS weight and range sizing segments 7-10

MISSION SIZING OR RANGE: AdvFtr_SFAwLT.dms.rdsdms

FPS		Enter analysis input parameters. For help click on column titles.					
7 WEIGHT DROP & TURNAROUND		8 COMBAT		9 CRUISE		10 CLIMB/ACCEL	
(n/a)	0.0	THRUST SETTING	Max	THRUST SETTING	100.	THRUST SETTING	100.
Weight DROPPED	5000.	ALTITUDE	15000.	ALTITUDE	15000.	STARTING ALT	15000.
(n/a)	0.0	VELOCITY	650.	VELOCITY	500.	END ALT	47000.
#DropExt.Stores	0.0	# TURNS	3.	RANGE	50.	START VEL	500.
Turnaround	Yes	(n/a)	0.0	Find Range	No	END VEL	660.53
BeginReserve	No	AlternatePolar#	0.0	AlternatePolar#	0.0	AlternatePolar#	0.0

Table 11 RDS weight and range sizing segments 10-13

MISSION SIZING OR RANGE: AdvFtr_SFAwLT.dms.rdsdms

FPS		Enter analysis input parameters. For help click on column titles.					
10 CLIMB/ACCEL		11 CRUISE		12 DESCENT		13 LANDING	
THRUST SETTING	100.	THRUST SETTING	100.	(n/a)	0.0	(n/a)	0.0
STARTING ALT	15000.	ALTITUDE	47000.	Wi/Wi-1	0.99	Wi/Wi-1	0.995
END ALT	47000.	VELOCITY	800.	RangeCredit	0.0	%Reserve&Trap	6.
START VEL	500.	RANGE	500.	(n/a)	0.0	(n/a)	0.0
END VEL	660.53	Find Range	No	(n/a)	0.0	(n/a)	0.0
AlternatePolar#	0.0	AlternatePolar#	0.0	(n/a)	0.0	(n/a)	0.0

Table 12 Fuel fraction results using RDS software

```
   MISSION SEGMENT          MISSION SEGMENT      Wi/WO      FUEL BURN     FUEL BURN    AIRCRAFT WEIGH
                            WEIGHT FRACTION                 -SEGMENT       -TOTAL      (end of Seg)
                            OR DROPPED WEIGHT                             (lbs-m)        49225.3
-------------------------------------------------------------------------------------------------
  1 TAKEOFF SEGMENT             0.9818            0.9818       894.6         894.6       48330.7
  2 CLIMB and/or ACCEL.         0.9739            0.9562      1262.0        2156.6       47068.7
  3 CLIMB and/or ACCEL.         0.8816            0.8430      5573.6        7730.2       41495.1
  4 CLIMB and/or ACCEL.         0.9755            0.8223      1017.9        8748.1       40477.2
  5 CRUISE SEGMENT              0.9531            0.7837      1897.7       10645.8       38579.5
  6 CRUISE SEGMENT              0.9811            0.7690       727.7       11373.5       37851.8
  7 WEIGHT DROP SEGMENT      5000.0000            0.6674         0.0       11373.5       32851.8
  8 COMBAT SEGMENT              0.9272            0.6188      2393.1       13766.5       30458.8
  9 CRUISE SEGMENT              0.9784            0.6054       657.3       14423.8       29801.5
 10 CLIMB and/or ACCEL.         0.9794            0.5929       614.9       15038.7       29186.6
 11 CRUISE SEGMENT              0.8171            0.4845      5336.8       20375.6       23849.7
 12 DESCENT SEGMENT             0.9900            0.4797       238.5       20614.1       23611.2
 13 LANDING SEGMENT             0.9950            0.4773       118.1       20732.1       23493.2
                                                     Reserve & trap =  1243.9
                                                        Total fuel = 21976.0
-------------------------------------------------------------------------------------------------
```

Table 13 Initial weight estimation iterations using RDS software

Iteration #	$W_{0,guess}$	W_E	W_F	$W_{0,calculated}$
1	60,000.0	23,869.6	27,116.7	57,256.3
2	57,942.3	23,332.2	26,135.0	55,737.2
3	49,517.5	21,058.7	22,115.5	49,444.2
4	49,227.6	20,978.2	21,977.1	49,225.3

To move forward to the wing loading (W/S) sizing, an initial weight was determined. The selected value will be used for the aircraft's wing loading (W/S) sizing. In comparison, both calculated takeoff weight values (W_{TO}) using Roskam's and Raymer's methods were acceptable values and comparable to the selected similar aircraft. Roskam's method calculated a much lower takeoff weight than Raymer's RDS software. One obvious difference was the reserve fuel that was included in the RDS calculation. Moreover, the strafe segment included in Roskam's method reduced the aircraft's weight significantly before performing the second supercruise segment, thus lowering fuel consumption. Additionally, RDS was able to calculate a combat segment in the mission profile, thus increasing fuel weight necessary for the completion of the mission. The RDS software provided more parameter inputs and segments compared to Roskam's method, therefore, it was determined that the RDS software takeoff weight (W_{TO}) result would be used for the aircraft wing and performance sizing.

3.3   Wing Loading and Performance Sizing Using Roskam's Method
3.3.1   Sizing To Stall Speed Requirements
According to MIL-C-005011B, there are minimum stall speed (V_{stall}) requirements. The required stall speed was determined from the values of the similar aircraft stall speed comparisons.

Determined stall speed (V_{stall}) requirement: 180 mph – 230 mph. The stall speed equation obtained from Roskam Eq. (3.3) was used to calculate the wing loading (W/S)$_{stall}$ necessary to meet the stall speed requirement.

Table 14 Similar Aircraft Stall Speed (V_{stall}) Comparison

	SU-15	F-14	F-15	MIG-29	MIG-31
V_{stall} (mph)	186.4	173	149.6	153	273 (estimate)

$$V_{stall} = \sqrt{\frac{2(W/S)}{\rho C_{Lmax}}} \qquad (3.3)$$

$$(W/S)_{stall} = \frac{1}{2}\rho\, V_{stall}^2 C_{Lmax} \qquad (3.4)$$

where, $C_{Lmax} = 1.2 - 1.8$

Table 15 Max Coefficient Values for Cruise, Takeoff, and Landing for 3 Types of Aircraft [24]

Aircraft Type	C_{Lmax}	$C_{Lmax,TO}$	$C_{Lmax,L}$
1. Military Trainers	1.2 – 1.8	1.4 – 2.0	1.6 – 2.2
2. Fighters	1.2 – 1.8	1.4 – 2.0	1.6 – 2.6
3. Supersonic Cruise Airplanes	1.2 – 1.8	1.6 – 2.0	1.8 – 2.0

In order to obtain an acceptable estimated values for sizing, similar aircraft data and data from Roskam [24] were used as baselines. For calculation of the stall speed (V_{stall}), Table 14 was used to estimate various speeds for a possible stall speed wing loading. The $C_{L,max}$ values were taken from Roskam [24], which included clean, takeoff, and landing configurations. The data ranges that were most important to investigate included military trainers, fighter, and supersonic cruise aircraft.
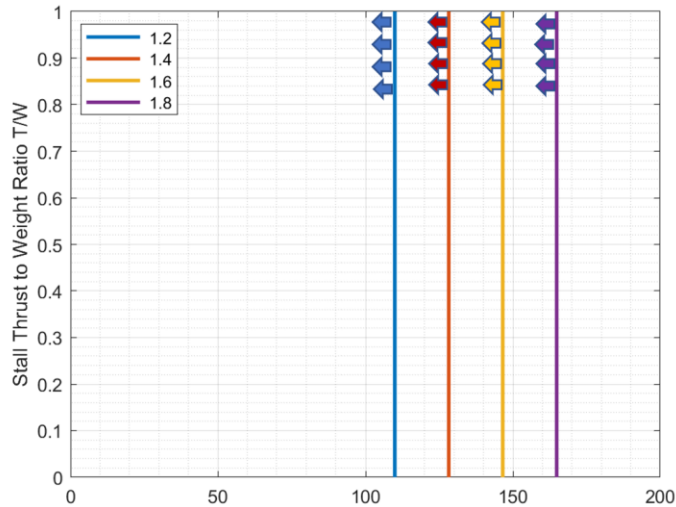
Figure 3 Calculated stall speed sizing for various C_{Lmax} values

The first parameter sized was the stall speed for various $C_{L,max}$ values obtained from Table 15. Figure 3 plots the stall wing loading (W/S) vs thrust-to-weight ratio (T/W). The graph showed four W/S values for the chosen $C_{L,max}$ values investigated. When the $C_{L,max}$ was 1.8, the maximum wing loading was at 165 lb/ft^2. This means, that the wing area for this $C_{L,max}$ was very small. According to Yang [26] benefits for having a high $C_{L,max}$, were shorter takeoff, lower minimum speed (stall speed) and lower noise level. However, high wing loading values were known to have used heavy and strong materials due to the wings' structural purposes.

3.3.2 Sizing to Take-off Requirements

As listed on the mission requirements, the aircraft must be able to perform a take-off ground roll of less than 2,500 ft and be able to fly at 50 ft above the take-off surface under 5,000 ft of horizontal distance or the take-off field length. Roskam's [24] take-off distance sizing method was used to calculate the wing loading, thrust-to-weight ratio, actual take-off ground run and take-off field length distances.
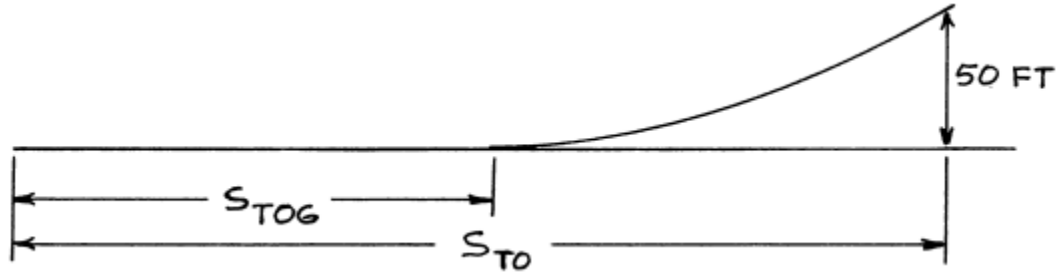
Figure 4 Take-off distances definition [24]

Equations 3.5 and 3.6 shown below calculated the required field length for an aircraft design. The field length equation included the wing loading, thrust-to-weight ratio and take off lift coefficient ($C_{Lmax,TO}$). The result of this equation sized the proper wing loading ranges to achieve the required field length.

Field length equation: $S_{TOFL} = (W/S)_{TO}/(\sigma\ C_{Lmax,TO}\ (T/W)_{TO})$ (3.5)

Ground run distance: $S_{TOG} = \dfrac{k_1\ (W/S)_{TO}}{\rho[C_{L,max,TO}\left(k_2\left(\left(\frac{T}{W}\right)_{TO}\right) - \mu_G\right) - 0.72 C_{Do}]}$ (3.6)

where: $k_1 = 0.0447$

$k_2 = 0.75\ \dfrac{(5+\lambda)}{(4+\lambda)}$ where: λ = engine bypass ratio

$\mu_G = 0.02 - 0.03$ ground (concrete) friction coefficient
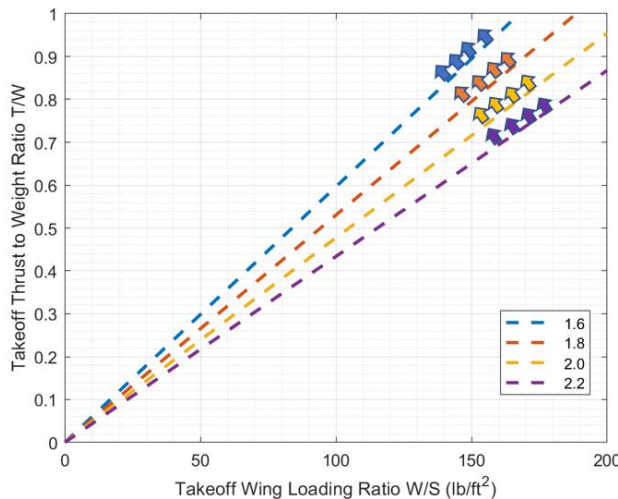
Figure 5 Calculated takeoff sizing for various $C_{Lmax,TO}$ values

This graph produced using Equation 3.6 showed how each takeoff lift coefficient related the wing loading and the needed thrust-to-weight ratio to achieve the required field length. The graph aligned with the previous claim by Yang [26], to which a high lift coefficient is best for shorter takeoff field lengths. Moreover, the graph showed that lower wing loading (bigger wing area) required less thrust. It seemed that with a $C_{Lmax,TO}$ of 1.6 required almost a thrust-to-weight ratio of 1:1.

3.3.3 Sizing to Landing Distance Requirements

The required distance for landing was limited below 5,000 ft over a 50 ft clearance height. Factors that determined the landing distance consisted of the landing weight W_L, Approach speed V_A, deceleration, flight qualities and pilot technique. The sizing for landing distance included the approach velocity calculation V_A. It was suggested to use the same method used for a FAR 25 landing distance sizing. The FAR 25 field length was defined as the total landing distance (S_L) divided by 0.6, where the 0.6 was considered the safety factor accounted for variations in pilot technique and other conditions. The one key difference for military fighter was the approach velocity equation. Also, the safety factor used for this sizing was 0.3, due to pilot experience and skillset.
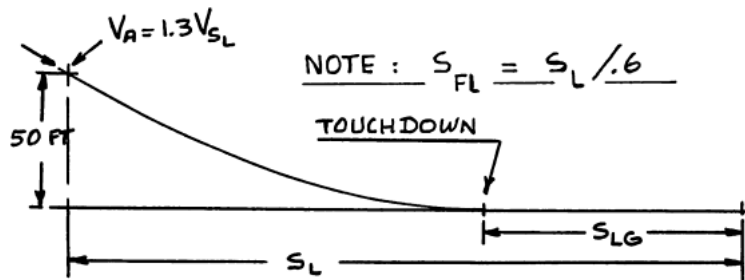
Figure 6 FAR 25 landing distance definition

Landing distance (land based) equation:

$$S_{FL} = 0.3V_A \qquad (3.7)$$

Approach speed (land based) equation:

$$V_A = 1.2V_{SL} \qquad (3.8)$$

where: V_{SL} = stall speed with landing configurations (gear, flaps, and power-off)
Using the stall speed Equation 3.4, the approach speed V_A was substituted for the stall speed V_{stall} in the equation.

$$[2(W/S)_L]/(\rho\, C_{L,max,L}) = V_A \qquad (3.9)$$

$$(W/S)_L = \frac{1}{2}V_A\, \rho\, C_{L,max} \qquad (3.10)$$

23
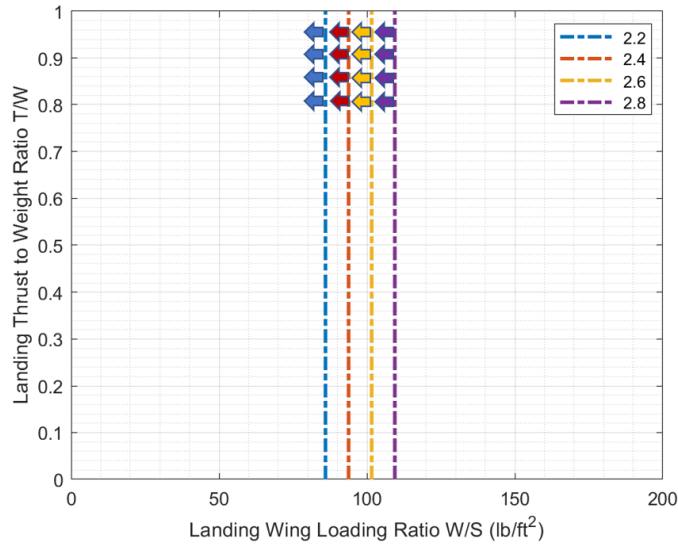
Figure 7 Calculated Landing W/S vs T/W Graph for Various $C_{Lmax,L}$ Values

The result for the landing distance sizing showed the limit for wing loading to achieve the required distance. The wing loading values were noticeably lower than the previous results. This was seen to be an alarming result, that led to the thought of changing the landing distance requirement. Even with the maximum $C_{Lmax,L}$ of 2.8, the wing loading was still limited to 110 lb/ft^2.

3.3.4 Sizing to Climb Requirements
In order to size an aircraft's climb performance, it was necessary to determine an estimated drag polar for the aircraft. Therefore, before sizing for the rate of climb of the aircraft, calculation of drag polars for subsonic and supersonic speeds were completed.

3.3.4.1 Drag Polar Estimation
Drag polar showed the relationship between zero-lift drag or more known as the parasitic drag (C_{Do}) and the induced drag (C_{Di}) and wave drag (C_{Dw}).

$$C_D = C_{Do} + C_{Di} + C_{Dw} \tag{3.9}$$

Parasitic drag can be expressed as:

$$C_{Do} = f/S \tag{3.10}$$

where f is the equivalent parasite area and S is the wing area.
Induced drag is the drag due to the lift force produced by any lifting surface of the aircraft and can be expressed as:

$$C_{Di} = \frac{C_L^2}{\pi Ae} \tag{3.11}$$

Lasty, wave drag is accounted for transonic and supersonic velocities. Since the mission requires super cruise, wave drag must be implemented in the drag polar estimation.
In can be expressed for a wedge shape wing as:

$$C_{Dw} = 4\left[\frac{\alpha^2+(t/c)^2}{\sqrt{(M^2-1)}}\right] \qquad (3.12)$$

Table 16 Fighter aircraft parasitic drag data provided from Roskam [24]

Parameter	F-14	F-18	F4C	X-3 Stiletto
Equivalent Parasite Area (ft²)	14	9	13	29
Wing Area (ft²)	565	400	530	166.5
Parasitic Drag Coefficient	0.025	0.0225	0.0245	0.174

The drag polar calculations parameters used for this polar sizing are gathered data from Roskam's and Raymer's aircraft design books.

Table 17 Drag polar parameter for drag polar calculation

Parameters	Take-off	Landing	Supercruise M=2.2 at AOA=5°	Supercruise M=1.4 at AOA=5°
Oswald's efficiency e	0.30	0.25	0.35	0.35
C_{Do}	0.050	0.135	0.03	0.03

The obtained initial drag polar of an aircraft helped determined the aircraft geometry, more specifically, its aspect ratio. Figures 8 and 9, shown below, were the results of drag polar estimations for; takeoff, landing, clean subsonic cruise, and clean supersonic cruise. The methods used were from Roskam's [24] sizing methods. It was important to determine these drag polar in order to size the rest of the parameter such as cruise, and climb rate. In the all figures below, the lowest aspect ratio (AR) of 3 produced the lowest C_L. Additionally, a wing aspect ratio of 3 produced the highest drag coefficient (C_D) for all configurations. It seemed that a higher AR such as 7 was far more superior when it came to aerodynamics. Lastly, the initial drag polar estimates for each configuration reached the highest lift coefficient ranges selected. This information helped determine the possible aircraft geometry for the design phase.
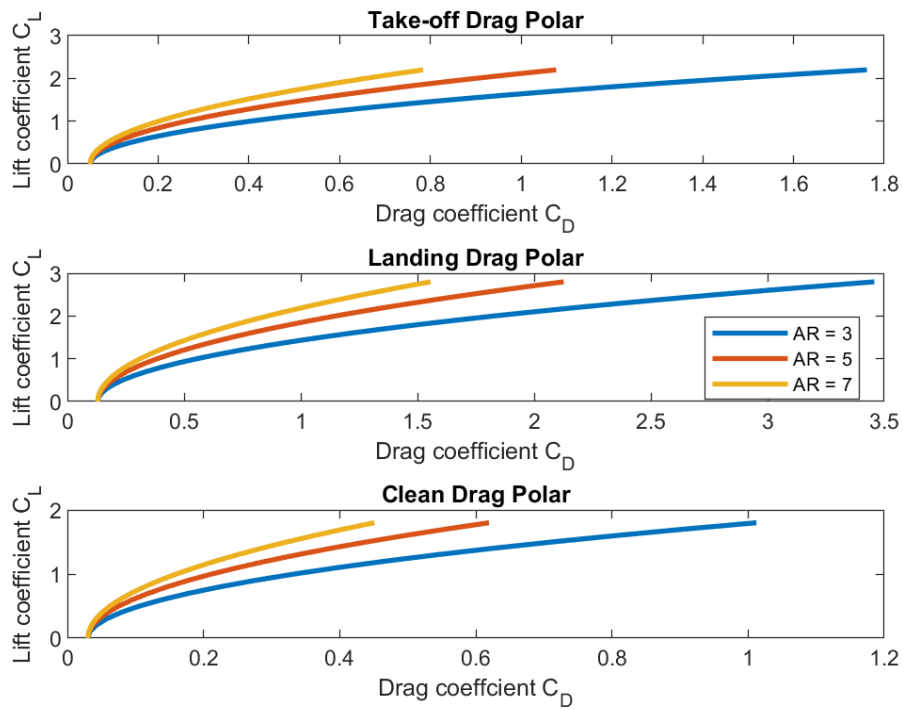
Figure 8 Calculated take-off, landing and clean (subsonic) drag polar with aspect ratio = 3,5,7
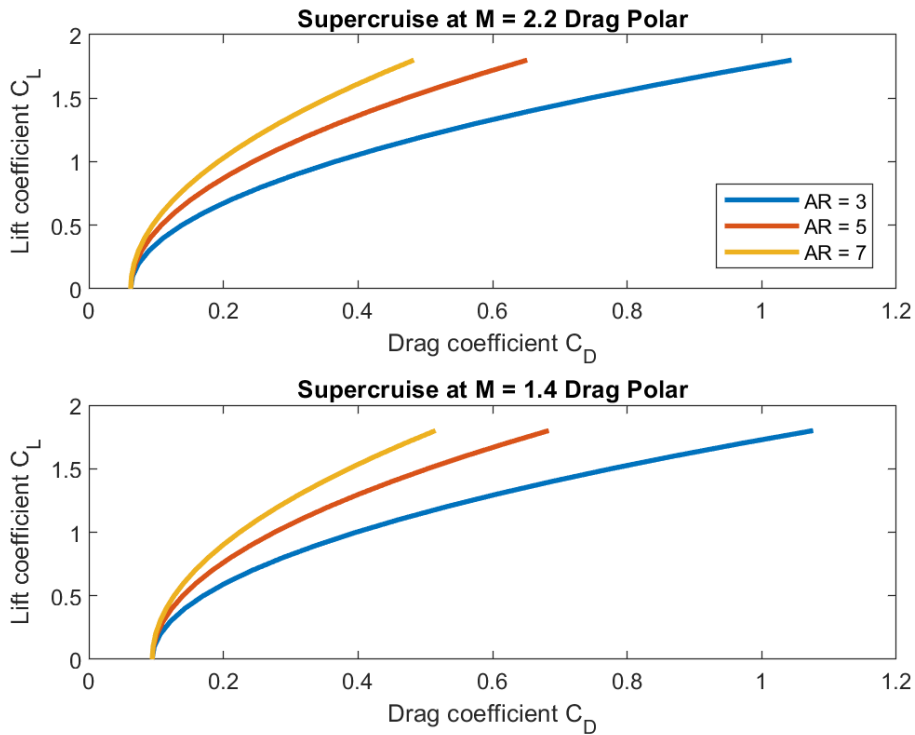
Figure 9 Calculated supercruise segment 5 and 12 at M = 2.2 and M = 1.4 drag polar with
A = 5°

3.3.4.2 Rate of Climb Calculation

The required rate-of-climb parameter (RCP) was a direct climb to 45,000 ft at maximum W_{TO} in 6 minutes. Also, the aircraft must climb from 45,000 ft to 50,000 at supersonic speed. The climb gradient required must be at least 0.045 or 250 ft/nmi.

Assumptions:
1. Specific excess power (P_s) must be above 100 ft/sec at 45,000 ft and M 0.85
2. Drag polar from the calculation above was used:
   Clean, low speed: $C_D = 0.03 + 0.302C_L^2$
   Clean, M = 1.7: $C_D = 0.0757 + 0.303C_L^2$
   Take-off, gear up: $C_D = 0.05 + 0.354C_L^2$

3.3.4.3 Climb Requirement 1): All Engines Operational Take-off gear up 2.) Engine out Take-off, gear up

This requirement of climb sizing involved one engine inoperative (OEI). The thrust-to-weight T/W and wing loading W/S ratios were tabulated for the best possible parameter that met the requirement.

For jet powered aircraft, the climb rate (RC) can be expressed as:

$$RC = V[(T/W) - 1/(L/D)] \tag{3.13}$$

Where V can be expressed as:

$$V = [2(W/S)/(\rho \ (C_{Do}\pi \ ARe)^{1/2})]^{1/2} \tag{3.14}$$

Maximum lift-to-drag ratio $(L/D)_{max}$ ca be expressed as:

$$(L/D)_{max} = \frac{1}{2}(\pi \ ARe/C_{Do})^{1/2} \tag{3.15}$$

Using Equations 3.12 through 3.14, the wing loading and thrust-to-weight ratio graph for OEI climb sizing was completed.
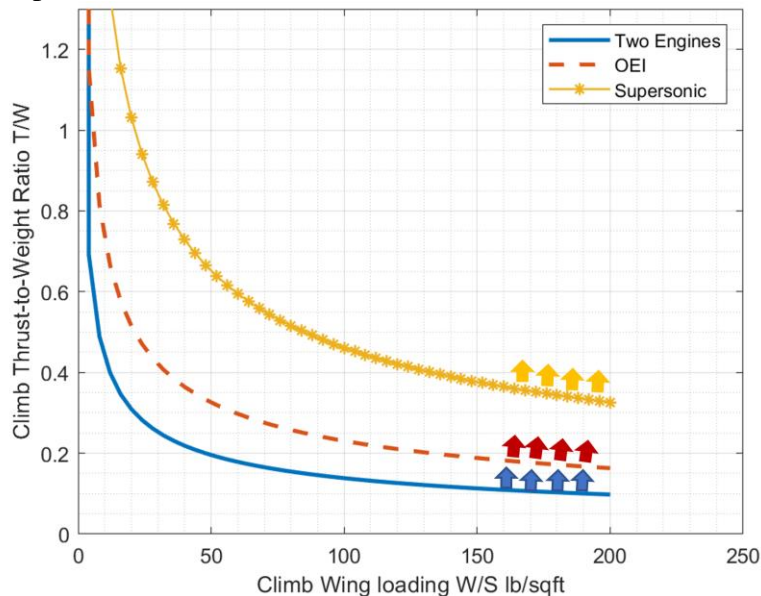
Figure 10 Climb rate sizing for two engines and one engine inoperative scenarios

The results from the rate-of-climb sizing plotted in Figure 10 The graph showed the wing loading and thrust-to-weight ratio relationship for the three aircraft climb configurations. It was noticed that low wing loading required less thrust-to-weight ratio for climb. It seemed that the

T/W for such climb gradient requirement was lower than expected. This meant, a climb rate that would better the requirement was possible.

3.3.5   Maneuvering Sizing Requirements

To be the superior aircraft, maneuverability characteristics during flight must also be superior. It allows the aircraft to outperform the enemy aircraft in many ways such as, turning and G load capacity. The requirements listed in the mission requirements were used to determine the proper sizing of the aircraft to perform there maneuvering requirements.

3.3.5.1 Load Factor Sizing

To be the superior aircraft, maneuverability characteristics during flight must also be superior. It allows the aircraft to outperform the enemy aircraft in many ways such as, turning and G load capacity. The requirements listed in the mission requirements were used to determine the proper sizing of the aircraft to perform there maneuvering requirements.

To reiterate the maneuverability requirements, include:
Turn rate $> 12°$ per second
Turn radius $< 4{,}500$ ft at 15,000 ft altitude
Load factor > 7 Gs, $V = 590$ kts at 15,000 ft altitude
Maximum load factor can be found from the equilibrium equation perpendicular to the flight path.

$$nW = C_L \bar{q}\, S = 1{,}482\delta\, M^2 C_L S \qquad (3.16)$$

$$n_{max} = (1{,}482 C_{L,max}\, \delta\, M^2)/(W/S) \qquad (3.17)$$

Using the Equation 3.18, the sizing was able to calculate the required thrust for a load factor.

$$T = C_{Do}\bar{q}\, S + (C_L^2/\pi\, ARe)\,\bar{q}\, S \qquad (3.18)$$

Thrust-to-weight ratio was calculated from rearrangement of this equation:

$$T/W = \bar{q}\, C_{Do}/(W/S) + (W/S)(n_{max})^2/\pi\, AR\, \bar{q} \qquad (3.19)$$

3.3.5.2 Turn Rate Sizing

Turn rate ($\dot{\varphi}$) was calculated with relation to the laod factor. The equation below expressed that the turn rate requirement must also meet the load factor requirement. This can be seen from equation Eq 3.19 shown below.

$$\dot{\varphi} = (g/V)(n^2 - 1)^{1/2} \qquad (3.20)$$

Since the turn rate was specified in the equation, equation Eq 3.19 was used to calculate if the required turn rate required an attainable and sustainable load factor.

$$N_{req} = [(V\dot{\varphi}/g)^2 + 1]^{1/2} \qquad (3.21)$$

28

Results from the sizing showed possible maneuvering performance that were considered basic for a fighter aircraft. Figure 11 was the generated plots for various turn rates from 12 degrees per second (deg/s) to 16 deg/s. The minimum requirement of 7 g's of load up to 9 g's of load were also plotted. According to the second graph, wing loading designs of less than 50 lb/ft^2 could achieve the 7 g's load and the 16 deg/s turn rate requirements with a thrust-to-weight ratio of 1. With wing loading above 100 lb/ft^2, the required thrust-to-weight ratio were more than 1. This meant that propulsion design must be considered to achieve such maneuvering capabilities.

Similarly, it was in the first graph that to achieve the required g load at high wing loading of more than 100 lb/ft^2, the thrust-to-weight ratio was mandatory be greater than 1. To reach a 9 g load during a maneuver smaller wing loading was considered the best option. Large wing areas such as in the F-15 and MIG-31 aircraft were known for their high load factor capabilities.
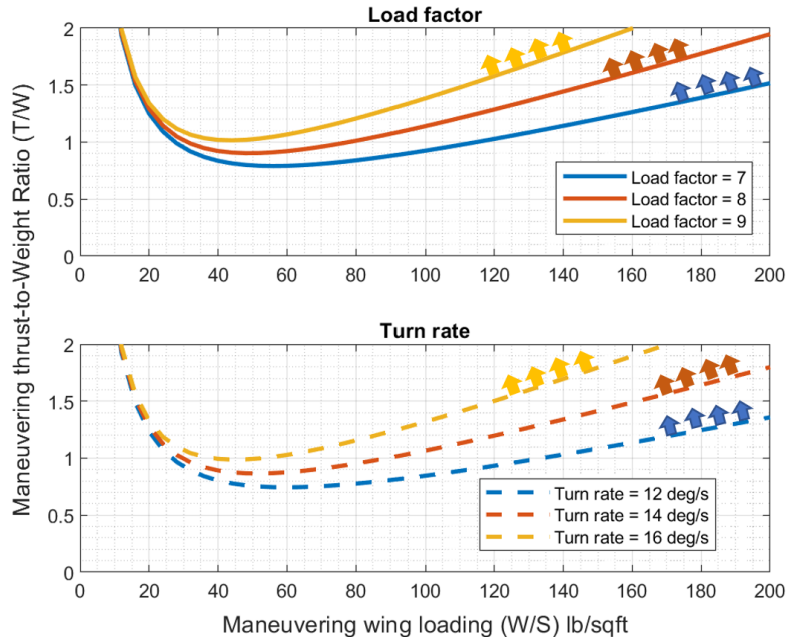
Figure 11 Maneuvering Requirements Sizing for load factor and turn rate

3.4 Cruise Sizing

The various cruise speeds of the aircraft were determined. During cruise flight, it was assumed that the required thrust was equivalent to drag, also the weight was equivalent to lift.

The cruise requirements include:
Supercruise (out): M = 2.2
Supercruise (in): M = 1.4
Cruise (dash): M = 0.88 at lower altitude

$$T_{req} = C_D \bar{q} \, S \qquad (3.22)$$

$$W = C_L \bar{q} \, S \qquad (3.23)$$

To size for cruise flight the thrust-to-weight ratio T/W and wing loading W/S equation was derived from Equation 3.57 and Equation 3.58.

$$(T/W)_{req} = C_{Do}\bar{q}/(W/S) + (W/S)\bar{q}\pi ARe \qquad (3.24)$$

For supersonic cruise flight:

$$(T/W)_{req} = C_{Do}\bar{q}/(W/S) + (W/S)\bar{q}\pi ARe + \bar{q}/(W/S)\,4\left[\frac{\alpha^2 + (t/c)^2}{\sqrt{(M^2-1)}}\right] \qquad (3.23)$$
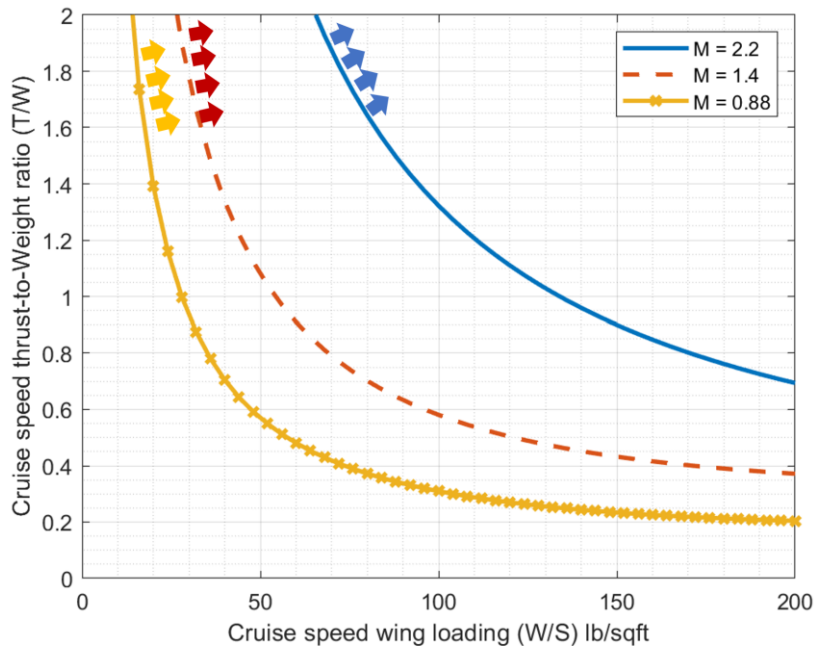
Figure 12 Cruise Speed Requirements Sizing for Segment 5,7,10,12

The last parameter sized was the cruise speed. The graph in Figure 12 nicely introduced the various sizing combinations to achieve the required speeds at for the mission's cruise segments. It was obvious that the fastest cruise speed of Mach 2.2 needed a high thrust-to-weight ratio at any wing loading. However, it was surprising to had seen that the difference in thrust-to-weight ratio and wing loading requirements between the speeds Mach 1.4 and Mach 0.8 was lower than expected. More importantly, the Mach 2.2 supercruise velocity seemed to be unattainable below wing loading of 100 lb/ft^2. Above this wing loading, the thrust-to-weight ratio was noticeably high. Further analysis helped with the realization of the difficulties that cruise speed requirements brought to the design.

3.5   Matching Graph
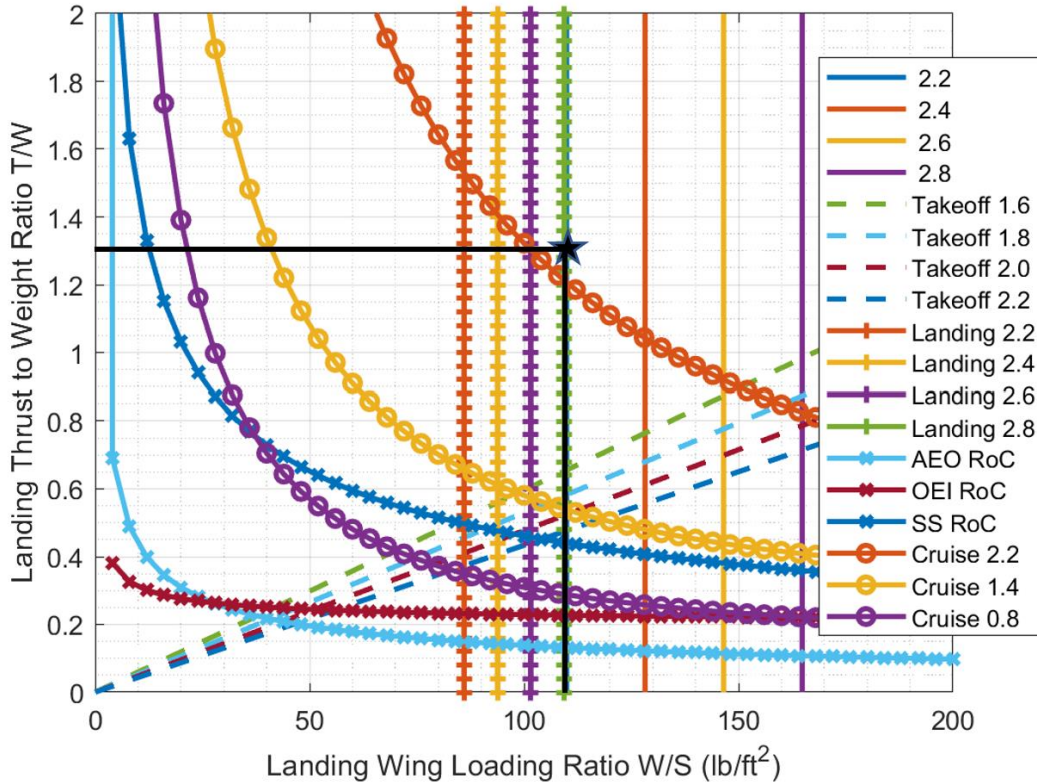
Figure 13 Matching graph sizing results

A potential thrust-to-weight ratio and wing loading was selected for the design. Figure 13 shows all the wing loading and thrust-to-weight ratio requirements for various segments that included; stall speed, takeoff, landing, climb rate and cruise speed. The selected value for the wing loading was 110 lb/ft^2 and thrust-to-weight ratio of 1.3. The main reason for such a thrust-to-weight ratio was due to the supercruise requirement of Mach 2.2. It was investigated, that increasing the cruise altitude to 65,000 feet would lower the T/W requirement to 1. A hesitation was decided to make these changes because, it was not investigated as to how increasing the ceiling affected the weight sizing of the aircraft. Further iteration was considered.

3.6   Discussion

Conducting the sizing for each mission requirements allowed better understanding of the limitations for this aircraft design. The initial weight estimation for the aircraft after performing Roskam's fuel fraction method showed comparable results against Raymer's RDS software. The estimated weights for both methods were accepted and deemed comparable against the selection of similar aircraft. The goal was to keep the aircraft take-off weight under 50,000 lbs. This goal was achieved after conducting the weight estimation.

Initial sizing was then conducted to create limitations for the aircraft parameters such as wing loading and thrust-to-weight ratio. The sizing included; stall speed, take-off and landing distance, rate-of-climb, maneuverability, and cruise speed. Each sizing was designed to meet the mission requirements that was placed for the aircraft. A stall speed requirement between 180 – 230 mph was placed, and can be achieved with various maximum lift coefficients. The results

showed that the highest possible wing loading can be achieved using a $C_{L,max} = 1.8$. Additionally, the take-off and landing distance requirements were used to determine the best wing loading, thrust-to-weight ratio maximum take-off and landing lift coefficients ($C_{Lmax,TO}$, $C_{L,max,L}$). It was seen that the sizing for landing required lower wing loading (W/S) than expected. Determination of the climb rate requirements provided significant data regarding the aircraft's climb performance. Three climb rates were calculated, a subsonic climb rate, a climb with one engine inoperative (OEI) and supersonic climb rate. It was obvious that the supersonic climb rate required higher thrust-to-weight ratio due its the drag polar characteristics.

Most importantly, the aircraft's maneuverability and cruise speed were sized according to the mission requirements. The required load factor of 7 G's and turn rate was seen to be easily achieved by the aircraft. However, the calculated results show high thrust-to-weight ratio (T/W) requirement for the aircraft design. The cruise speed sizing was to investigate the various wing loading (W/S) and thrust-to-weight ratio (T/W) for various cruise speeds for the aircraft. The segment for Mach 2.2 super cruise required the highest thrust-to-weight ratio (T/W) out of the three speeds. However, this supercruise requirement was found to be achievable with a high wing loading (W/S) which would require lower thrust-to-weight ratio (T/W).

3.7   Conclusion

Up to this point, the aircraft design will move forward once the wight loading and thrust-to-weight ratio that satisfies all requirements have been selected. It was previously discussed that the aircraft weight estimates were acceptable and comparable against the similar aircraft selection. Each mission requirements seem achievable as long as the selected wing loading, thrust-to-weight ratio, and maximum lift coefficients are within the requirements of the aircraft's missions. Selection of these parameters allows the performance sizing to take place. This sizing is to ensure that the selected parameters are verified to meet the aircraft's performance requirements and performance optimization. Further analysis needs to be done to improve for the best selection of wing loading and thrust-to-weight ratio. More importantly, the requirements may also change if it provides great difficulties in the design. Tradeoffs are a big part design; therefore, all must be considered to complete the best aircraft design.

3.8   RDS Initial Aircraft Performance Analysis

For comparison purposes, a performance sizing was conducted using an alternate method by Raymer's design software called RDS. The performance analysis was determined using the aircraft data from the weight and range analysis. The analysis covered aircraft performance such as takeoff, landing, climb/acceleration, and maneuvering. The results were able to produce the lift coefficients and thrust-to-weight ratios for each mission segment selected. The aircraft wing loading was a parameter input in the aircraft data used for the RDS performance analysis. The wing loading nominated from the matching graph shown in Figure 3.12 was used for the analysis. The analysis was able to analyze the nominated wing loading of 110 lb/ft^2.

Table 18 RDS aircraft data (U.S standard units)

T/W, W/S, and Weights		Misc. Design & Aero Data		[M#] Stores Drag [D/q]	
T/W (Takeoff)	1.3	#Engines	2.	0.0	0.0
W/S (Takeoff)	110.	Nmax	8.	0.0	0.0
Wo-Drawn	47218.5	q-max	2200.	0.0	0.0
We-Drawn	20417.4	CLmax-TO *	1.7033	0.0	0.0
Wcrew	220.	CLmax-Lnd *	2.8	0.0	0.0
Wcargo	6270.	CL-ground *	0.1	0.0	0.0
Wpassenger	250.	LandingGear Cd*	0.01	0.0	0.0
Wmisc UL	0.00001	Braking Cd *	0.002	0.0	0.0
Woil	50.	(n/a)	0.0	0.0	0.0
We Coeff C	-0.3475	(n/a)	0.0	0.0	0.0
Parasite Drag	Induced Drag	CLmax &CLalpha	Thrust - Max	C at Max T	T - dry|econ
	Available Wfuel = 20011.1 lbs-m		T~total=61384.05 S=429.3		

The parameters shown in Table 18 were used for the performance analysis of the initially sized aircraft. As previously stated, the wing loading along with the thrust-to-weight ratio were taken from the matching graph. The weights used were the weight results from the RDS initial weight sizing. Moreover, the different $C_{L,max}$ values from the matching graph was also used as inputs for the aircraft data.

3.8   Performance Parameters

The RDS software performance analysis provided its users the choice to determine which performances was analyzed. The figures below were the actual parameters used for this aircraft's performance analysis.

Table 19 RDS performance sizing parameters (takeoff, dash-out climb/accelerate, excess power and turns with two engines)

PERFORMANCE: AdvFtr_SFAwLT.rdsdpa

FPS	Enter analysis input parameters. For help click on column titles.						
1 TAKEOFF		**2 CLIMB**		**3 ACCELERATE**		**4 Ps & TURN**	
Wi/Wo or Wi	0.98	Wi/Wo or Wi	0.9736	Wi/Wo or Wi	0.865	Wi/Wo or Wi	0.6036
Altitude	0.0	Start Altitude	0.0	Altitude	50000.	Altitude	15000.
Obstacle Height	50.	End Altitude	45000.	Start Vel or M#	1.7	Velocity or M#	0.95
Rolling Coeff	0.03	Velocity or M#	0.85	End Vel or M#	2.1	Thrust Setting	Max AB
CL-ground *	0.0	Thrust Setting	100.	Thrust Setting	Max AB	One Engine Out	No
CLmax-T.O. *	0.0	Extra delta Cd	0.0	Extra delta Cd	0.0	Extra delta Cd	0.0
Time to Rotate	1.	(n/a)	0.0	(n/a)	0.0	(n/a)	0.0
GEAR Cd *	0.0	(n/a)	0.0	(n/a)	0.0	(n/a)	0.0
Thrust Setting	100.	(n/a)	0.0	(n/a)	0.0	(n/a)	0.0
Braking Coeff	0.3	(n/a)	0.0	(n/a)	0.0	(n/a)	0.0
Braking Cd *	0.0	%Stall Margin	0.0	%Stall Margin	0.0	%Stall Margin	0.0
#DropExtStores	0.0	#DropExtStores	0.0	#DropExtStores	0.0	#DropExtStores	0.0
(n/a)	0.0	(n/a)	0.0	(n/a)	0.0	(n/a)	0.0
(n/a)	0.0	(n/a)	0.0	(n/a)	0.0	(n/a)	0.0
AlternatePolar#	0.0	AlternatePolar#	0.0	AlternatePolar#	0.0	AlternatePolar#	0.0

Parameters for the takeoff, subsonic climb to 45,000 feet of altitude, acceleration to super cruise, and excess power and maneuvering turns (Ps & turns) were contained in Table 19. Proper weight fractions were obtained from the initial weight sizing and inputted in the parameters in order to produce a more accurate analysis. It can be seen in the table that maximum thrust with afterburners were used for acceleration and maneuvering performances. A significant information about the Ps & turns segment must be mentioned. This segment focused on the occasion to which the aircraft had only one engine operational.

Table 20 RDS performance sizing parameters (dash-in climb/accelerate, landing)

PERFORMANCE: AdvFtr_SFAwLT.rdsdpa

FPS	Enter analysis input parameters. For help click on column titles.						
4 Ps & TURN		**5 CLIMB**		**6 ACCELERATE**		**7 LANDING**	
Wi/Wo or Wi	0.6036	Wi/Wo or Wi	0.5816	Wi/Wo or Wi	0.5816	Wi/Wo or Wi	0.4839
Altitude	15000.	Start Altitude	15000.	Altitude	47000.	Altitude	0.0
Velocity or M#	0.95	End Altitude	47000.	Start Vel or M#	0.8	Obstacle Height	50.
Thrust Setting	Max AB	Velocity or M#	0.8	End Vel or M#	1.4	Braking Coeff	0.3
One Engine Out	No	Thrust Setting	66.	Thrust Setting	100.	CL-ground *	0.0
Extra delta Cd	0.0	Extra delta Cd	0.0	Extra delta Cd	0.0	CLmax-Landing *	0.0
(n/a)	0.0	(n/a)	0.0	(n/a)	0.0	Braking Delay	1.
(n/a)	0.0	(n/a)	0.0	(n/a)	0.0	Gear Cd *	0.0
(n/a)	0.0	(n/a)	0.0	(n/a)	0.0	Braking Cd *	0.0
(n/a)	0.0	(n/a)	0.0	(n/a)	0.0	T-rollout/fwd	0.0
%Stall Margin	0.0	%Stall Margin	0.0	%Stall Margin	0.0	Vtd/Vstall	1.1
#DropExtStores	0.0	#DropExtStores	0.0	#DropExtStores	0.0	#DropExtStores	0.0
(n/a)	0.0	(n/a)	0.0	(n/a)	0.0	(n/a)	0.0
(n/a)	0.0	(n/a)	0.0	(n/a)	0.0	(n/a)	0.0
AlternatePolar#	0.0	AlternatePolar#	0.0	AlternatePolar#	0.0	AlternatePolar#	0.0

Table 20 included the climb segment after the aircraft combat/weapons drop/ground assault segment. Moreover, the table included the dash-in supercruise, which had a lower velocity than of the dash-out supercruise velocity. Additionally, this supercruise segment was analyzed at a lower supercruise altitude. The main reasoning for the lower altitude was to limit the fuel burn during climb-in segment.

Table 21 RDS performance sizing parameters (excess power and turns with one engine, dash-out climb)

FPS		Enter analysis input parameters. For help click on column titles.					
6 ACCELERATE		7 LANDING		8 Ps & TURN		9 CLIMB	
Wi/Wo or Wi	0.5816	Wi/Wo or Wi	0.4839	Wi/Wo or Wi	0.6036	Wi/Wo or Wi	0.88
Altitude	47000.	Altitude	0.0	Altitude	15000.	Start Altitude	45000.
Start Vel or M#	0.8	Obstacle Height	50.	Velocity or M#	0.965	End Altitude	50000.
End Vel or M#	1.4	Braking Coeff	0.3	Thrust Setting	Max AB	Velocity or M#	1.4
Thrust Setting	100.	CL-ground *	0.0	One Engine Out	Yes	Thrust Setting	100.
Extra delta Cd	0.0	CLmax-Landing *	0.0	Extra delta Cd	0.0	Extra delta Cd	0.0
(n/a)	0.0	Braking Delay	1.	(n/a)	0.0	(n/a)	0.0
(n/a)	0.0	Gear Cd *	0.0	(n/a)	0.0	(n/a)	0.0
(n/a)	0.0	Braking Cd *	0.0	(n/a)	0.0	(n/a)	0.0
(n/a)	0.0	T-rollout/fwd	0.0	(n/a)	0.0	(n/a)	0.0
%Stall Margin	0.0	Vtd/Vstall	1.1	%Stall Margin	0.0	%Stall Margin	0.0
#DropExtStores	0.0	#DropExtStores	0.0	#DropExtStores	0.0	#DropExtStores	0.0
(n/a)	0.0	(n/a)	0.0	(n/a)	0.0	(n/a)	0.0
(n/a)	0.0	(n/a)	0.0	(n/a)	0.0	(n/a)	0.0
AlternatePolar#	0.0	AlternatePolar#	0.0	AlternatePolar#	0.0	AlternatePolar#	0.0

Finally, Table 21 ended the analysis with another Ps & turns segment, but with all engines operational. Furthermore, the landing segment was analyzed to determine if the current aircraft performance meet the landing field length requirements.

3.8.1 Performance Results
3.8.1.1 Takeoff Performance Analysis
The takeoff performance analysis provided specific distances during the takeoff segment. Like the takeoff distance analysis using Roskam's method, the FAR 25 air worthiness standards. More information was determined using the RDS performance analysis. The results included performances such as the ground roll, rotate, and transition distances. More importantly, the takeoff field length required was determined. If recalled from Chapter 2, it was stated that the ground run must be less than 2,500 feet at sea level and the field length must be no greater than 3,000 feet. The results for the takeoff analysis shown below in Table 3.19.

Table 22 Aircraft takeoff performance analysis using RDS

Performance parameter		Distance (ft)	
Wing loading (W/S)	107.8 lb/ft^2	Ground roll	1,158.2
Thrust-to-weight ratio (T/W)	0.902	Rotate	253.84
Stall speed	157.3 mph	Transition	1,043.6
Maximum lift coefficient ($C_{L,max,TO}$)	1.191	Total takeoff	2,455.6
Takeoff speed	180 mph	FAR 25 AEO takeoff	2,824
Obstacle height	50 ft	Balanced field length	2,833.2

The results shown in Table 22 meets all the takeoff mission requirements. The analysis resulted in a much lower takeoff distance than the requirement. Moreover, the ground roll distance result was less than half of the requirement. The wing loading and the thrust-to-weight ratio were well under the limiting values. Notably, the stall speed result from the analysis was surprisingly much lower than the required range was 180 mph – 230 mph.

3.8.1.2 Climb Performance Analysis

The climb performance analysis consisted of two aircraft mission segments. The first analysis was the initial climb segment where the starting altitude was at sea level, and end altitude of 50,000 feet. For this segment, the climb was divided to two climbing procedures. A subsonic climb was done from sea level to 45,000 feet with ending velocity of Mach 0.85. Another climb procedure was analyzed from 45,000 feet to 50,000 feet, where the climb included an acceleration from Mach 0.85 to Mach 1.4. The second climb analysis was to climb at the dash-in supercruise altitude. This segment's starting altitude was at 15,000 feet and end altitude of 47,000 feet. This climb stayed at subsonic speed of Mach 0.8.

Table 23 Climb performance analysis results for both climb segments

Performance	Sea level to 45,000 ft	45,000 ft to 50,000 ft	15,000 ft to 47,000 ft
Wing loading W/S (lb/ft$^{2)}$	107.1	96.8	63.976
Maximum thrust-to-weight ratio T/W	1.007	0.28	0.707
Maximum climb rate (ft/min)	48,970	5,106	29,423
Climb distance (nmi)	25.89	22.51	21.54
Climb gradient (ft/nmi)	1,738	222	1,485
$C_{L,max}$	1.906	1.086	1.967
Climb time (min)	3.10	1.68	2.77

The climb segments' performances gathered from the RDS method achieved mission requirements. Shown in Table 23 was the data from the analysis. The climb performances were analyzed for each climb procedure. The table shows that climbing from sea level to 45,000 feet produced the best climb performance at about 50,000 ft/min. However, the thrust-to-weight ratio required for this climb was one to one. It was great achievement to know that supersonic climb from 45,000 feet to 50,000 feet was attainable. The climb gradient result was less than the mission requirement of 250 ft/min, however, this was still an acceptable performance due to the supersonic climb speed. Most importantly, both climb segments were under 6 minutes, which was a stated mission requirement for climb.

3.8.1.3 Maneuverability Performance Analysis

The maneuverability analysis consisted of two performances, load factor and turns. As a fighter aircraft, the maneuverability performances were intended to match or better the maneuverability of the selected similar aircraft. The analysis was conducted to determine how the aircraft perform during combat, weapons drop and ground attack. Moreover, the analysis determined the aircraft maneuverability for all engines operating (AEO) and one engine inoperative (OEI). It was of great importance to determine if the aircraft was still able to perform within the mission requirement for maneuverability even with one engine inoperative.

Table 24 Aircraft maneuverability performance analysis for AEO and OEI at 60 percent M_{TOW}

Performance Parameter	All engines operating (AEO)	One engine inoperative (OEI)
Wing loading W/S (lb/ft^2)	66.396	66.396
Thrust-to-weight ratio T/W	1.88	0.94
$C_{L,max}$	1.77	1.75
Maximum turn rate (deg/s)	14.6	12.5
Maximum turn radius (ft)	3,950	4,670
Maximum load factor n	8	7
Specific excess power Ps (ft/s) at maximum load factor	586.82	5.71
Climb rate at n = 1 (ft/min)	100,881	42,346

The maneuverability performance analysis data entailed that the current sizing of the aircraft was able to achieve most of the mission requirements. In Table 24, a low wing loading can be seen. This was because, at that segment, the fuel fraction was at 60 percent of the maximum load. This allowed its peak maneuverable performance during the most important segment of the mission. With all engines operating, a whopping 1.88 thrust-to-weight ratio is available during this segment. This allowed a topmost maneuvering performance of achieving a 14.6 deg/s turn rate, less than 4,000 feet turn radius and load factor of 8 g's.

In contrast, Table 24 portrayed that even at EOI aircraft configuration, a .94 T/W ratio was available. The performance of this configuration, the aircraft was able to manage a 12.5 deg/s turn rate and 4,670 feet turn radius. Its turn radius performance was not met the requirements; however, it was able to achieve a load factor of 7 g's. It was safe to assume that the aircraft's maneuverability performance was comparable to the similar aircraft, and met the requirements.
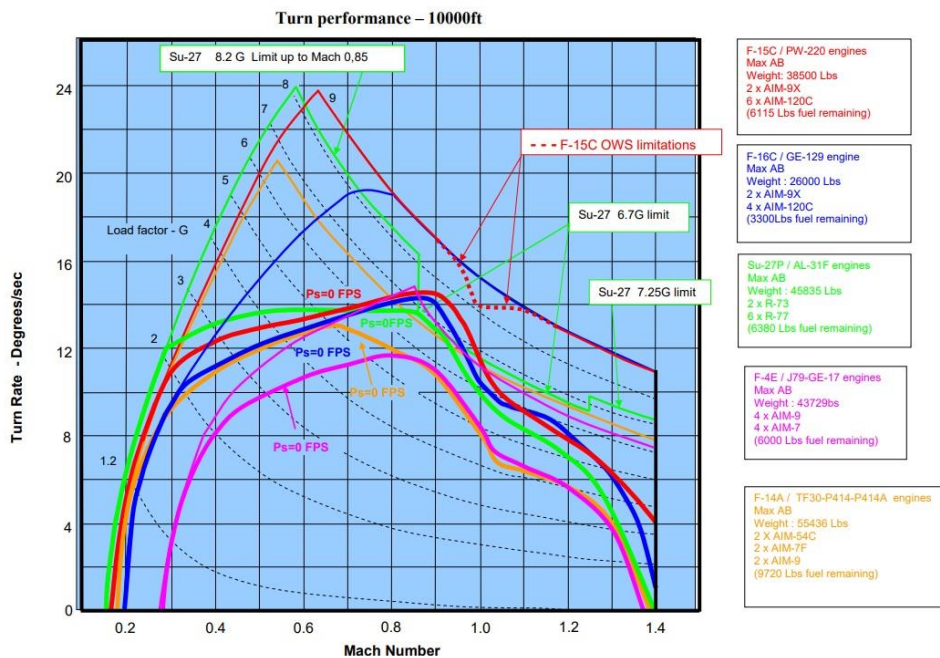
Figure 14 Similar aircraft maneuverability comparison

3.8.1.4 Landing Performance Analysis

Lastly, the aircraft's landing performance concluded the aircraft sizing chapter. RDS software performed the analysis to determine the aircraft's landing capabilities. It was important to know if the analyzed landing performances were able to achieve the mission requirements for this segment. Parameters such as the approach velocity, approach angle were provided in the results of the analysis. However, the main performance in check was the landing distance under FAR 25 and the ground roll distance. A breakdown on the performance was listed in Table 25.

Table 25 verified that the selected W/S and T/W were very much capable of performing greater than the landing requirements. In the table, the total landing distance under FAR part 25 was easily below the 5,000 feet requirement, and a ground run of below 2,500 feet. Important details such as the touchdown speed and landing stall speed were listed in the table. These values seemed lower than the known landing velocities of other fighter aircraft. A hypothesized reason for the low landing speed results were due to the low landing weight which was 48 percent of the M_{TOW}.

Table 25 Aircraft landing performance under FAR Part 25

Parameter		Distance (ft)	
Wing loading (W/S)	53.23 lb/ft^2	Approach	867.8
Thrust-to-weight ratio (T/W)	0.0	Flare	172.7
Stall speed	74.94 mph	Braking	1005
Maximum lift coefficient ($C_{L,max,TO}$)	2.52	Total ground roll	1,144
Landing touchdown speed	100 mph	Total distance	2,184.7
Obstacle height	50 ft	FAR 25 landing	3,641.2

3.8.2   Conclusion

The following performance analysis proved that the selected wing loading and thrust-to-weight ratio from the wing sizing matching graph performed within the mission requirements. It was verified that using a W/S of 110 lb/ft^2 was able to achieve takeoff under the maximum limit of ground roll and takeoff field length. Moreover, this wing loading performed way beyond expectations for the climb segment. It was able to produce high performances in climb gradient, time of climb, and rate of climb. The maneuvering aspects determined that with all engines operational, the selected wing loading was able to achieve high load factors, above average turn rate, and small turn radius. The performance analysis also exhibited achievable acceleration from high subsonic/transonic speed to supersonic speeds. Most importantly, the landing performance was remarkable. The analysis determined astounding landing stall speed, touchdown speed, and total field length landing distance. The sizing has been determined acceptable. Additionally, the performance analysis of the current sizing results confirmed that the mission requirements were achievable with proper design.

4.0   Configuration Design

4.1   Overall Configuration

The overall configuration determined the aircraft classification. There were many aircraft classifications that produced various overall configuration. For this aircraft design, a conventional over all configuration was selected. Roskam [27] offers various fighter aircraft overall configurations for comparison. Table 26 listed the overall configurations of interest for the design. Each overall configurations are designs to meet their requirements. The three overall configuration in considerations were the conventional configuration, flying wing configuration, and canard configuration.

Table 26 Aircraft overall configurations of interest for the design
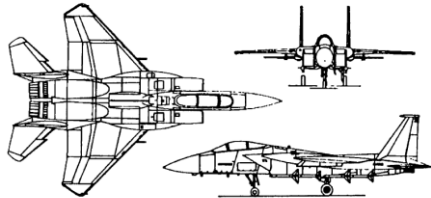
Conventional overall configuration
b) MCDONNELL DOUGLAS F-15C EAGLE

Flying wing (delta wing) overall configuration
d) GENERAL DYNAMICS F-16XL   c) DASSAULT-BREGUET MIRAGE III-E
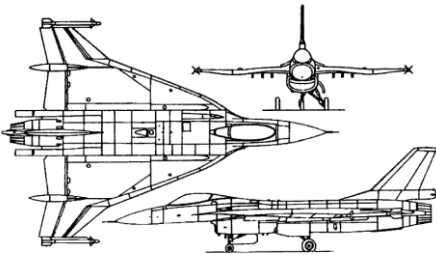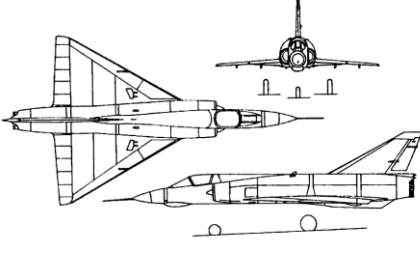
Canard overall configuration
d) SAAB JA 37 VIGGEN
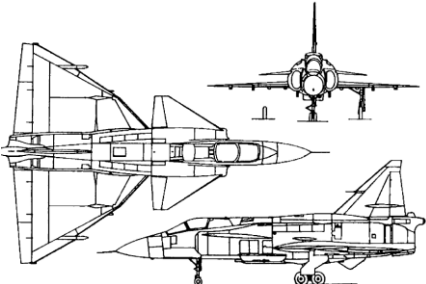
4.2   Fuselage Configuration

There were many types of fuselage configuration presented in Roskam's design book such as conventional fuselage, twin fuselage, or the Bernelli [27]. For this design, the best option for the fuselage configuration was the conventional configuration. Important geometrical parameters were investigated for this fuselage design. Table 27 was formed from Roskam's list airplane types geometric parameters. The ratios listed in the table was defined by the notations from Figure 15.
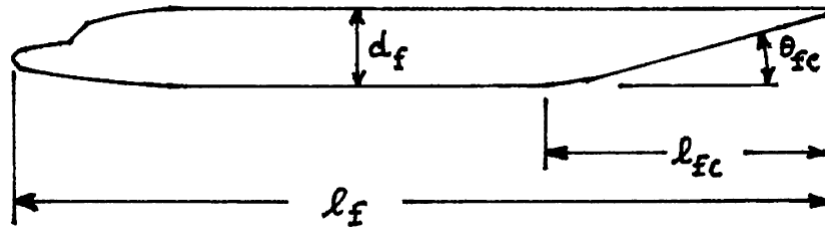
Figure 15 Geometric definitions of fuselage parameters [27]

Table 27 Geometric fuselage parameters for fighters and supersonic transports [27]

Airplane type	l_f/d_f	l_{fc}/d_f	θ_{fc}
Fighters	7 - 11	3 - 5°	0 - 8
Supersonic Transports	12 – 25	6 – 8	2 - 9

Table 27 provided data of ratios for the geometric design of the aircraft's fuselage. The first parameter was the length-to-diameter ratio l_f/d_f. This ratio played an important role in the past designs for low-boom research aircraft. The next two parameters provided fineness ratio. These ratios were described to had effects on base and friction drag, weight, and takeoff and landing rotations.

To adhere the low boom requirement, an additional parameter y_f/L modifies the fuselage nose bluntness. According to Darden's theory, this parameter must have values between 0.04 and 0.08 [28]. Figure 27 portrays the parameter y_f/L of a low boom aircraft configuration. This parameter is the ratio between the nose bluntness and the over length of the aircraft. As literature suggests, the nose bluntness ratio $y_f/L > 0.1$.
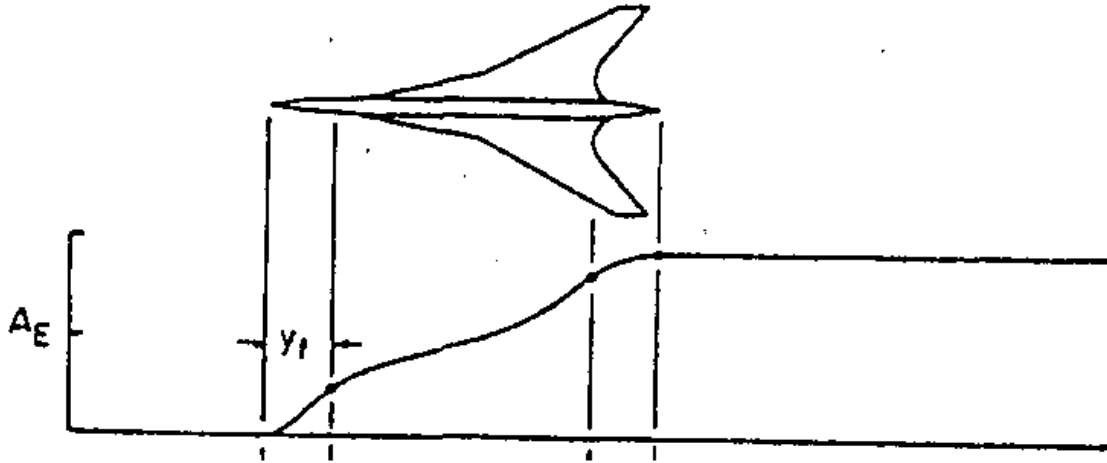
Figure 16 Nose bluntness parameter y_f/L to modify conventional fuselage for low boom configuration

4.3   Propulsion System and Integration

The configuration process involves the determination of the proper propulsion system for the aircraft. It must meet all the performance requirements such as cruise and maximum speeds, operating altitude and range.
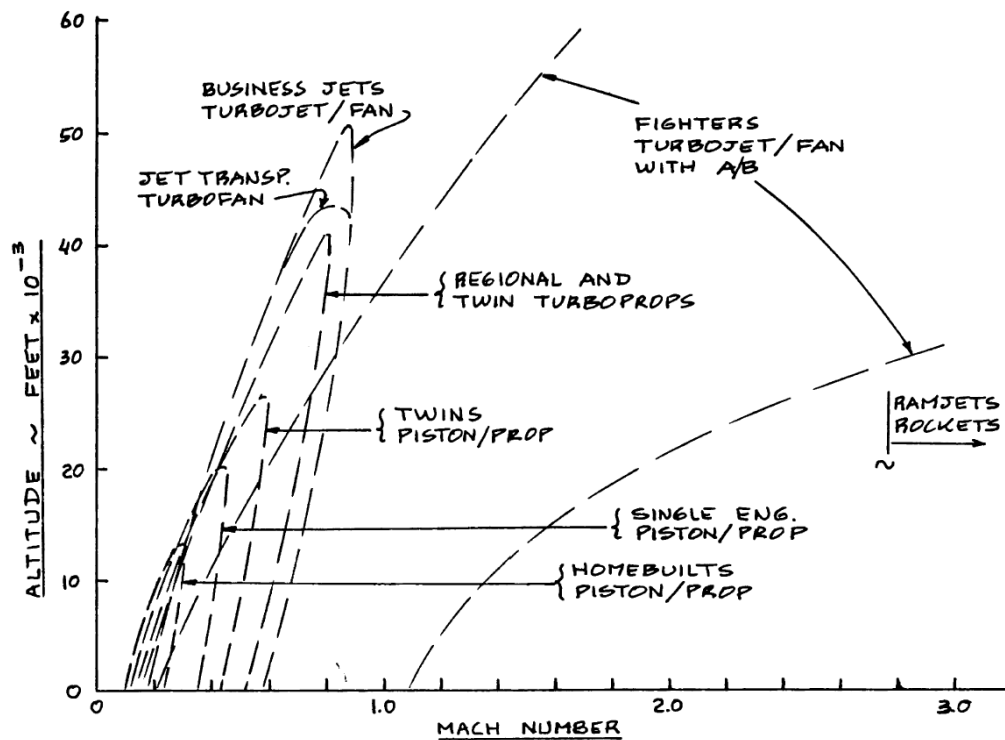
Figure 17 Speed-altitude envelope for various engine types of an airplane

A useful data to determine the type of engine for the aircraft is shown in Figure 17. The figure provides an envelope of engine types in relation to altitude and speed. It is obvious that for this design, the proper engine for the propulsion system is a turbojet or turbofan engine with

41

afterburners. These types of engines cover a flight envelope from speeds from Mach 1.0 to Mach 2.8, and operating at altitudes of 30,000 ft up to 60,000 ft.

Propulsion integration includes the selection of the number of engines and the thrust of each engine. According to Roskam [27], two possibilities are proposed for engine selection. First, a development of a new engine specifically designed to meet the mission requirements and performance sizing of the aircraft. Second, using an existing engine with available data that meets the requirements. For this design, the latter is selected for the propulsion system. Existing engines are sufficient to meet the mission requirements stated in chapter 2. More importantly, the sizing results require thrust levels achievable using two engines. A design study by Lockheed and Boeing -- relating the probability of engine failure and the number of engines used -- shows that for two engines, a probability for a one engine failure is doubled. For a two-engine failure however, the probability is squared. Therefore, the lower the probability of an engine failure for a two-engine aircraft, the less likely for both engines to fail.

4.4   Wing Configuration

The selection of the wing configuration for this aircraft design follows Roskam's "Procedure for wing planform design and for sizing and locating lateral control surfaces" section of his book [27]. This method determines; the overall structural wing configuration, wing-to-fuselage location, wing planform, and control surfaces.

Geometric data are taken from Roskam [27], to help determine the baseline for the wing planform. Tables 28 and Table 29 show geometrical data and overall wing configurations of fighter aircraft and supersonic cruise aircraft. The selection for this aircraft's configuration is a combination of these data and from current low-boom research data.

Low-boom research data shows that most of the wing configuration used were cantilever configurations with low and mid wing placements. The research claims that a reconfigured Northtrop-Grumman F-5 fighter aircraft was designated as a demonstrator for NASA [27]. Additionally, more current low-boom aircraft configurations shown in Figure 18, also has cantilever wings with low wing-to-fuselage arrangement.

The wing configuration selection begins with the overall wing-to-fuselage structural configuration. For this aircraft, the cantilever wing configuration best fits. A cantilever structure produces less drag compared to other configurations such as a braced wing. Next is the wing arrangement. Data from the low-boom research shows that past quiet supersonic demonstrators used low and mid wing configurations. However, the selected wing arrangement for this design is a high wing configuration. Roskam's data [27] from Table 28 reveals that two of the 5 similar aircraft, the F-14 and F-15 have high wing configuration. Since the two aircraft are known to be successful fighter aircraft, adding the low-boom effect during a supersonic cruise segment.

Wing planform configuration consists of wing sweep, taper, dihedral/anhedral and incident angles. Wing sweeps are necessary for supersonic flight. The wing planform inspiration is from the F-16 XL cranked-arrow delta wing. Additionally, low-boom supersonic aircraft configuration shown in Figure 18 use wing sweeps, more specifically cranked-arrow delta wing as well. It is noted that one disadvantage of a delta wing is the inability to use a trailing edge flap type of high lift devices. This makes wing design for achieving high lift coefficient much more difficult. Moreover, it initiates the use alternate high lift devices and techniques such as leading-edge flaps or slats.

(a) Side view of aircraft (b) Front view of aircraft

(c) Top view of aircraft (d) Oblique view of aircraft
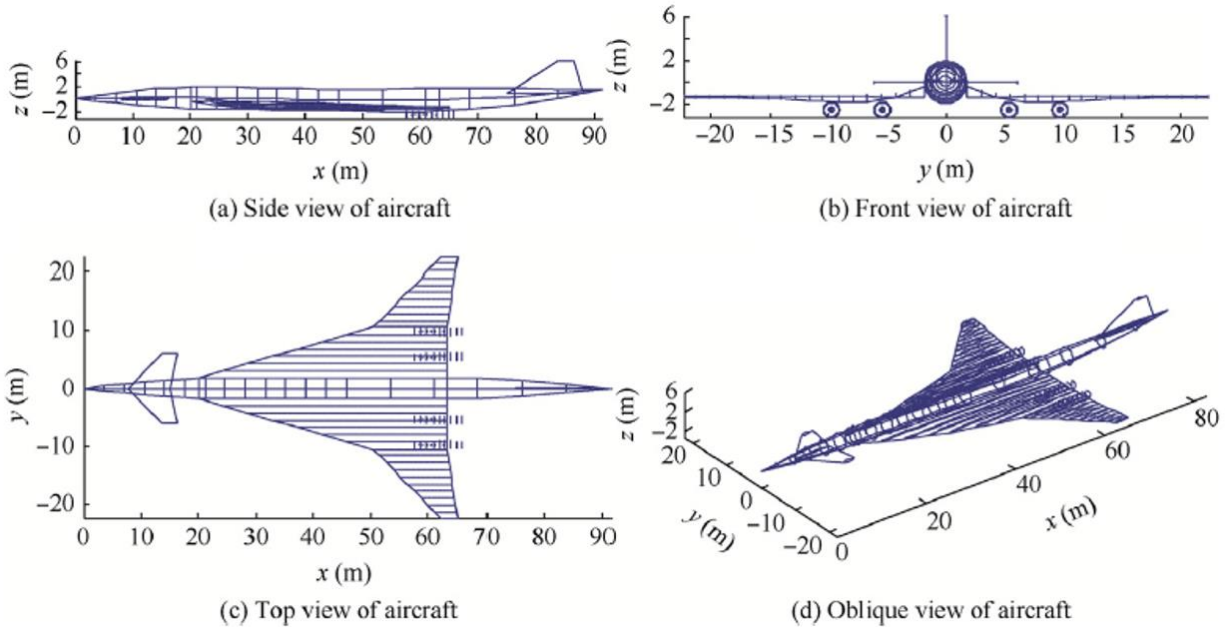
Figure 18 Example of one of various low-boom supersonic aircraft configurations

Table 28 Fighter aircraft wing geometrical data [27]

Type	Dihedral Angle, Γ_w, deg.	Incidence Angle, i_w, root/tip deg.	Aspect Ratio, A	Sweep Angle, $\Lambda_{c/4}$, deg.	Taper Ratio, λ_w	Max. Speed, V_{max}, kts	Wing Type
DASSAULT BREGUET							
Mirage III-E	-1	0	1.9	61(LE)	0	1,268(39K)	ctl/low
Mirage F1-C	-4.5	NA	2.8	48(LE)	0.29	1,260	ctl/shldr
Mirage 2000	-1	NA	2.0	58(LE)	0	1,260	ctl/low
Super Etendard	-3.5	NA	3.2	45	0.50	573	ctl/mid
Fairch.R.A-10A	7 (outer)	-1	6.5	0	0.66	450	ctl/low
Grumman A-6E	0	NA	5.3	25	0.30	700	ctl/mid
Grumman F14A	-1.5(out)	NA	7.3*	20/68(LE)	0.40	M = 2.4	vsw/high
Northrop F-5E	0	0	3.8	24	0.19	710	ctl/low
Vought A-7E	-5	-1	4	35	0.25	595(5K)	ctl/high
McDONNELL DOUGLAS							
F-4E	0/12	NA	2.8	45(LE)	0.18	1,146	ctl/low
F-15	-1	0	3.0	39	0.25	M =2.5	ctl/high
AV-8B	-12	1.8	4.0	24	0.28	585(0K)	ctl/shldr
GD FB-111A	0	NA	7.6*	16/73(LE)	0.33	1,260	ctl/shldr
GD F-16	0	0	3.0	40(LE)	0.22	495(33K)	ctl/mid
Cessna A37B	3	3.6/1	6.2	0	0.68	455	ctl/low
Aerm. MB339K	2.6	NA	5.3	8.5	0.58	500	ctl/low
Sukhoi Su-7BMK	0	NA	2.6	62(LE)	0.26	730(0K)	ctl/mid

ctl = cantilever   shldr = shoulder   (30K) = 30,000 ft altitude
* taken at lowest sweep angle

Table 29 Supersonic cruise aircraft wing geometric data [27]

Type	Dihedral Angle, Γ_w, deg.	Incidence Angle, i_w, root/tip deg.	Aspect Ratio, A	Sweep Angle, $\Lambda_{c/4}$, deg.	Taper Ratio, λ_w	Max. Speed, V_{max}, kts	Wing Type
NORTH AMERICAN AVIATION (ROCKWELL)							
XB-70A	-3	NA	1.8	65.6(LE)	0.02	M = 2$^+$	ctl/low
RA-5C	0	NA	4.0	37.5	0.19	1,204(40K)	ctl/high
B-1B	0	NA	??	??	0.32	M = 2$^+$	ctl/low
BOEING							
SST	NA	NA	3.4*	30-72	0.21	1,565(75K)	ctl/low
AST-100	get data from NASA reports						
NASA							
SSXJet I	0	NA	1.84	72(LE)	0.08	M =	ctl/
SSXJet II	0	NA	1.84	72(LE)	0.08	M =	ctl/
SSXJet III	0	NA	1.84	72(LE)	0.08	M =	ctl/
TUPOLEV							
Tu-144	8.3 (out)	NA	1.9	76/57	0.13	1,350(50K)	ctl/low
Tu-22M	0	NA	8.0*	20-65	0.28	1,446	ctl/mid
Dassault MIVA	-1.5	NA	1.8	60(LE)	0.11	1,261(36K)	ctl/low
GD F-111A	0	NA	7.5*	16-72	0.33	1,432$_+$	ctl/high
GD B-58	0	NA	2.2	59(LE)	0	M = 2$^+$	ctl/low
Aerospatiale/British Aerospace							
Concorde	0	NA	1.7	ogive	0.12	1,259(55K)	ctl/low

```
ctl = cantilever    (30K) = 30,000 ft altitude
* taken at lowest sweep angle
```

4.5   Empennage Configuration

The next configuration selection covers the empennage of the aircraft. The empennage consists of the horizontal and vertical stabilizers. These stabilizers are exactly just that. The empennage produces counter lift forces against the wings and freestream of air to stabilize the aircraft.

For this aircraft, it is important to emulate the similar aircraft or the basic fighter aircraft configurations. The is because, fighter aircraft are meant to be maneuverable, thus have much lower stability characteristics than the current low-boom commercial jet configurations. Therefore, the selection for this aircraft is a twin vertical stabilizer and a horizontal stabilizer attached to the delta wing. It is often configured together with the delta wing since the wing sweeps all the way to the tail of the fuselage. With this configuration, the aircraft obtains characteristics as a wing-body. A great example of this configuration is the F-16XL, Mirage III, and JA-37 shown in Table 28.

Additionally, using two vertical stabilizers are beneficial in both aerodynamics and safety. Two vertical stabilizers avoid the vortices being produced by the wing fairings, thus have better flow to produce more lift. Also, having a second vertical stabilizer acts as a redundancy factor for safety in case one encounters a failure. However, two vertical stabilizers does have negative effects on the aircraft such as increased weight due to using two actuators, and may require a more complex control system design.

4.6   Landing Gear Configuration

The completion of the aircraft configuration ends with the landing gear configuration selection. There are not as many selections for this of aircraft. The landing gear system uses

retractable gears, for obvious aerodynamic reasons. According to Roskam [27], a fixed or non-retractable gear produces unnecessary high amounts of drag force. Moreover, a conventional configuration (nosewheel or tricycle) configuration is the best choice for such aircraft.

4.7 Proposed Configuration Draft

A sketch of the overall configuration is shown in Figure 19. The figure shows the three different views of the aircraft. The top view shows the left half side of the aircraft. The sketch of a normal configuration of a fighter aircraft. The added nose length is for the low-boom configuration much like the F-5 design from Benson's configuration [27]. Moreover, the proposal follows the area rule, where the fuselage thickness decreases at the wing section of the aircraft. This proposal consists of the cranked-arrow delta wing with two vertical stabilizers. Also, a tricycle landing gear configuration is added in the sketch. Lastly, a two-engine configuration is implemented for the propulsion system of the sketch.
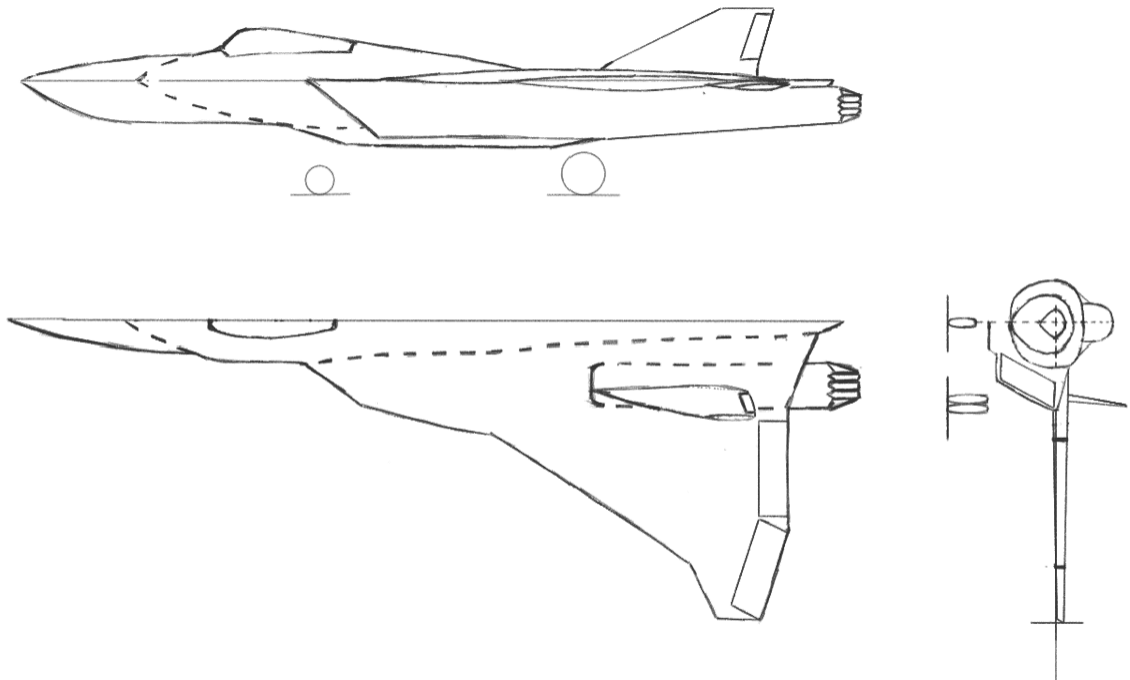
Figure 19 Overall proposed configuration for SFAwLT aircraft

5.0   Fuselage Design

5.1   Fuselage Packaging

The fuselage design begins with determining the equipment and components and crew within the aircraft. For this preliminary conceptual design, the basic equipment and components will be included. The goal for the packaging design is to ensure a structurally sound, well balanced, and aerodynamics of the aircraft [24]. Each of these component placements must be configured properly. Table 30 lists the equipment and components that are inside the aircraft.

Table 30 Aircraft fuselage components and equipment [6]

Component/equipment	Type
Radar	Active electronically scanned array (AESA)
Avionics	BAE systems
Automatic cannons	V61 Vulcan 20 mm
Ammo	1,000 lb drum
Missiles	Air intercept missiles (AIM)
Pilot seat	N/A

5.2   Cockpit Design

Two important things to consider in cockpit design for a fighter jet, visibility and ergonomics. Fighter aircraft rely on being able to see their surrounding when flying in the air. Therefore, the cockpit design must adhere to the acceptable parameters for fighter aircraft cockpits. Since this aircraft is a one-man crew, meaning one pilot aircraft, the F-16 aircraft provides a good inspiration in what the cockpit visibility should be. Figure 20 shows the angles of visibility the pilot must see from the cockpit. In this figure, an angle of 15° between the pilot's line of sight and the aircraft's nose angle is the forward visibility. This angle is much more difficult to achieve with the low-boom configuration, since lengthening the nose decreases the boom effects of the aircraft.

More importantly, the cockpit design must consider canopy drag. A large canopy provides great pilot visibility, however, produces high canopy drag. A stream more streamlined canopy produces less drag, but compromises pilot visibility. The cockpit design considers these options. The resulting design incorporated the 15° forward visibility while achieving a small and streamlines canopy. Table 32 lists the cockpit design dimensions including the canopy angle and visibility angles.

Figure 20 Cockpit visibility angle and inboard profile [27]

Next is the design of an ergonomic cockpit. This involves proper seat placement, flight controls accessibility and movement space. Figure 21 from Roskam shows the seating position of a pilot in a fighter aircraft along with the dimensions of the flight controls. The values for each marked dimension are provided in Table 20.

Figure 21 Pilot seating and center stick flight control dimensions

Table 31 Seating arrangement dimensions measured in inches [27]

A	B	C	D deg.	E deg.	F	G	H	I
41	30	5	19	101	29.75	10	14.50	19

J	K	L	M	N	O	P	Q	R
6	9	17	36	5	9.25	15	7	25

Seat adjustment: horizontal: ± 2.50 in. and vertical: ± 3.50 in.

Table 32 Fuselage cockpit dimensions

Cockpit components	Volume (ft^3)	Length (in)	Width (in)	Height (in)
Pilot seat	20.4	43	20	41
Side panel flight controls	3.4	19	16	19.25
Canopy clearance	N/A	N/A	N/A	3
Overall cockpit	23.4	52	40	56

Cockpit visibility	Elevation	Azimuth
	25°	134°

5.3   Weapons Integration Design

For the fuselage design, it is also important to safeguard the armaments the aircraft is equipped with. The weapons bay can have many effects on the aircraft such as weight and balance, stability and control and aerodynamics. Using internal weapons bay greatly benefits they aircraft's aerodynamics versus externally mounted weapons. The weapons bay design includes the design of the bay doors, aerodynamic components, and armament placements. The aircraft is required to carry at least six to ten missiles internally; therefore, the design of the weapons bay must be able to accommodate the maximum number of missiles. To address the unsteady flows as the bay doors open, a study at Cranfield University reports that cavity shaping modifies the shear layers inside the cavity and reduce noise levels. Table 33 shows the dimensions of the weapons bay and internal cavity.

Moreover, the internal cannon has significant effects on the stability and control of the aircraft. The recoil of the canon must be considered in the design. According to Roskam [29], the shoulder mounted cannons – as is in the F-15 – optimum location eliminates its negative effects on the aircraft's stability and aerodynamics.
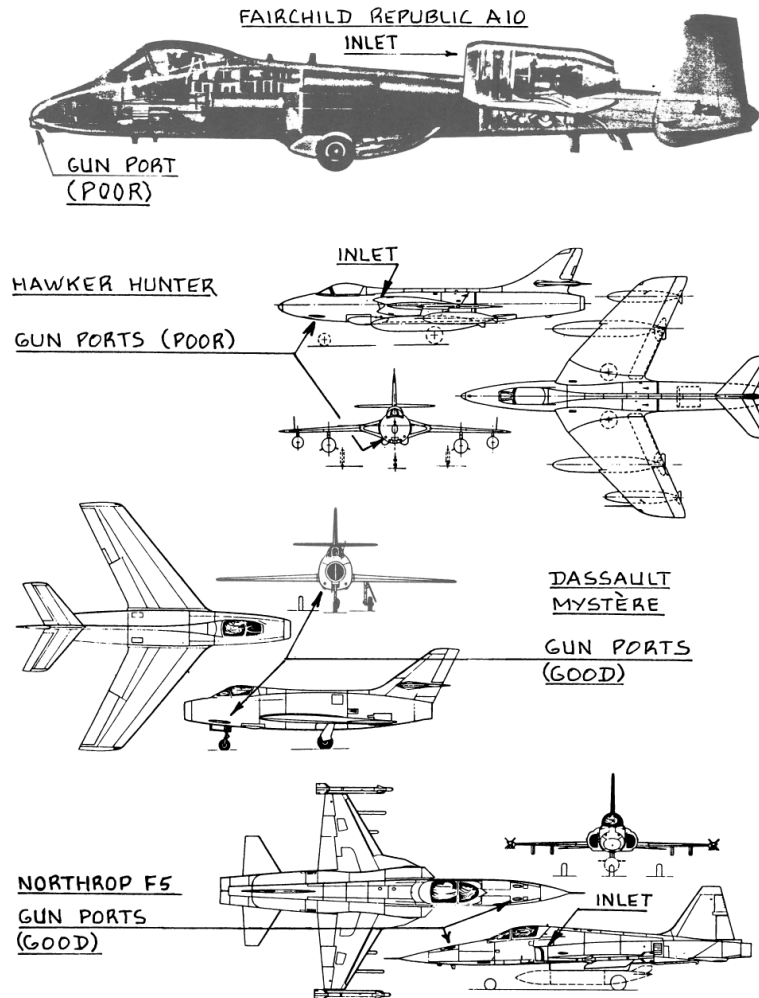
Figure 22 Examples of poor and good cannon locations for fighter aircraft [29]

Table 33 Weapons storage dimensions

Armament	Location	Volume (ft^3)	Length (ft)	Width (ft)	Height (ft)
Automatic cannon	Shoulder	N/A	6	2	2
Ammo drum	Aft cockpit	128	8	4	4
Short range AIM	Forward bay	79.275	10.5	3.02	2.5
Mid-range AIM	Aft bay	290.175	18.25	5.3	3
Long range AIM	Conformal storage	128.659	13	3.125	3.17

5.4   Fuselage Layout Design

The fuselage layout design determines its profile base, and compressibility drag. The aft body fineness ratio, upsweep angle and corners design as seen in Figure 23 can add or reduce fuselage drag. These geometries produce separated vortices thus increasing drag and can cause lateral oscillation issues [29]. Compressibility drag is greatly affected by the fuselage longitudinal shape. To design for an acceptable compressibility drag, the area rule must be determined along the length of the fuselage.

Secondly, adjustment of the fuselage design to decrease the sonic boom production of the aircraft is applied. The design initiates with the fuselage equivalent length to height of the spike ratio (H/L). Figure 24 illustrates the F-function plot with respect to the fuselage x-coordinate. The mission profile states that the supersonic cruise altitudes are 50,000 ft at Mach 2.2 and 47,000 ft at Mach 1.4. The design incorporates studied values of h/L = 6.0 and h/L 5.0 from previous studies on low boon designs [30]. Also, the same study suggests values for the nose bluntness $y_f/L = 0.02 - 0.08$. This value determines the desired fuselage length that achieved the low boom pressure profile. Figure 25 exhibits analytical graphs from previous studies of a low boom design.
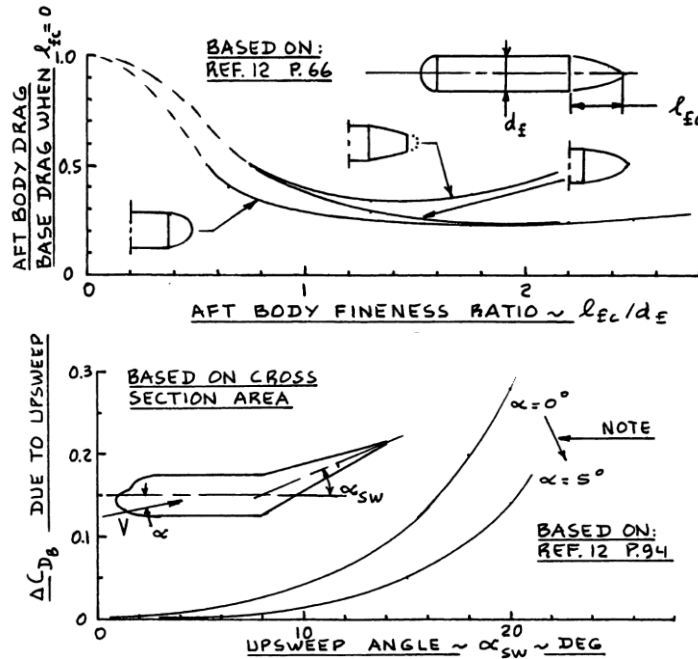
Figure 23 Aft body fineness ratio and upsweep angle plots versus base drag [29]
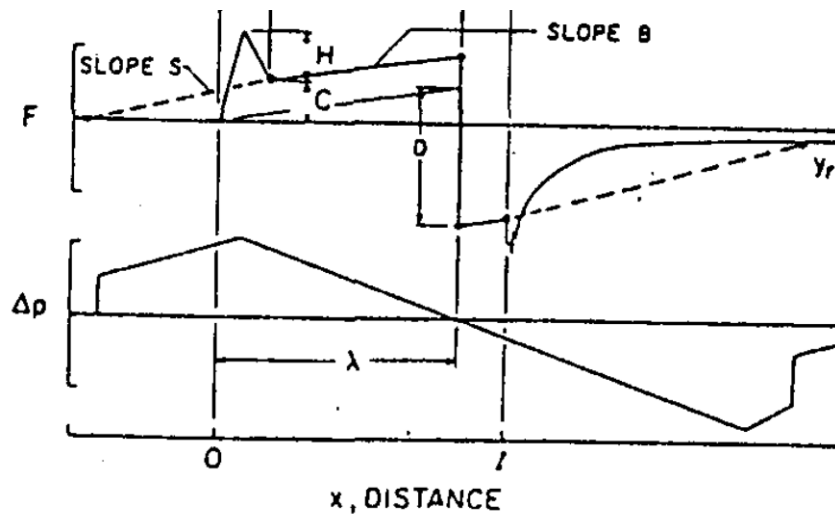
Figure 24 F-function graph for low boom concept [27]
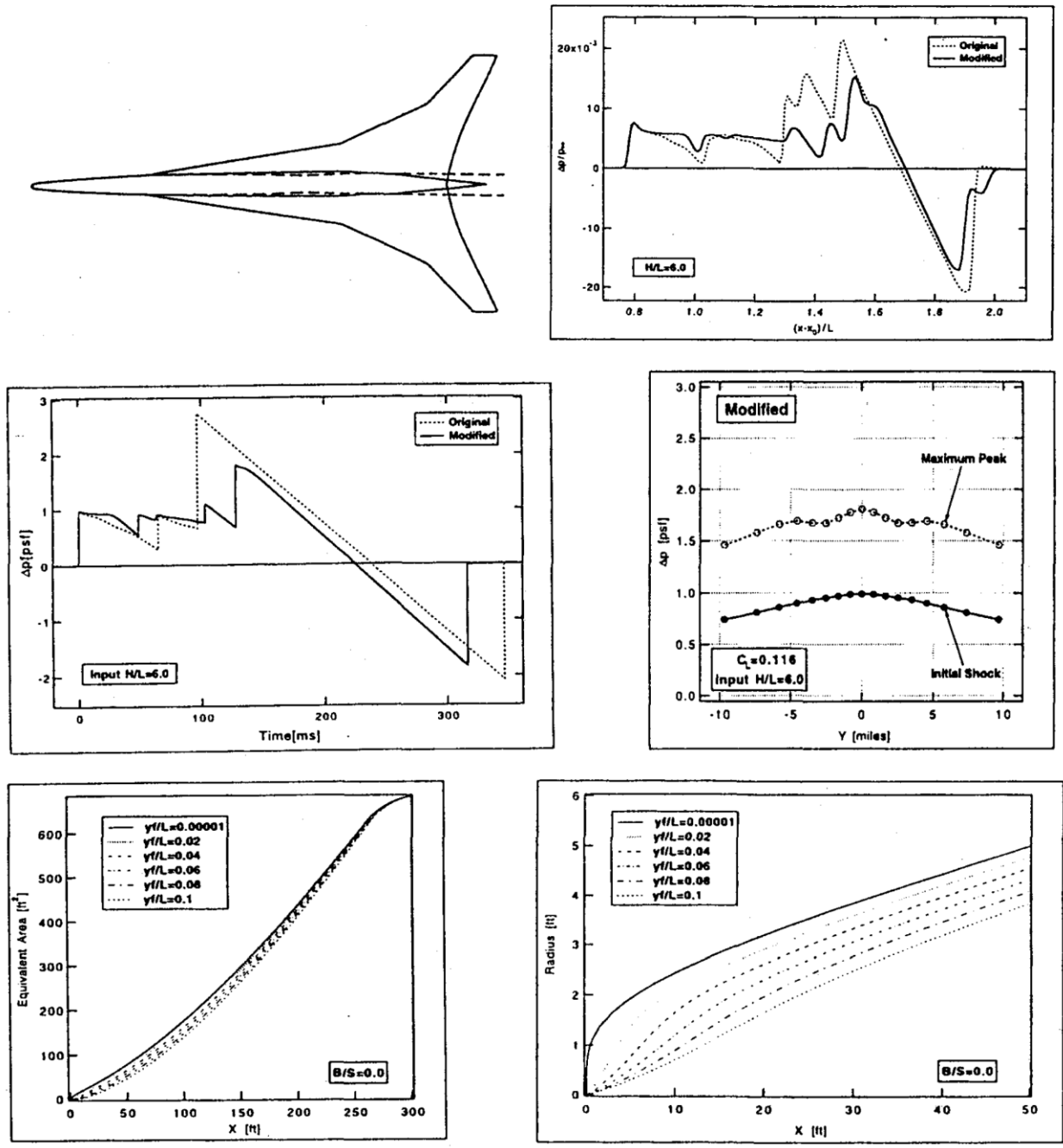
Figure 25 Low boom analytical results for equivalent area regarding effects of blunt nose design
[30]

Table 34 Fuselage layout dimensions with low boom geometric application

l_f (ft)	d_f (ft)	l_f/d_f	l_{fc} (ft)	l_{fc}/d_f	θ_{fc} (deg)	α_{sw} (deg)	y_f/l_f	y_f (ft)	H/l_f	H (ft)
65	4	16.25	17.7	4.425°	8°	8°	0.04	2.6	6	390

5.5 Discussion

The design of the fuselage implements the low boom configurations from previous x-planes and current low boom supersonic transport aircraft designs. Section 5.1 lists the typical loads of a fighter aircraft. The cockpit design applies for a one seat pilot with the basic flight control equipment and an ejection seat. The estimated total volume of the cockpit is about 24 ft³. The design uses the dimensions provided data from Roskam's book [27].

Furthermore, the fuselage design for the weapons storage allows an internal weapons bay enough to carry up to 8 missiles and an automatic cannon. The largest missile stored are long range air-to-air missiles located in the conformal storage. A great deal of planning for storage placement are necessary in order to fit all of the armaments internally. The length of the fuselage allows the weapons bay suitable to carry all the missiles. It is unusually longer than any other fighter aircraft. More importantly, the weapons bay design implements internal cavity shaping to decrease aerodynamic disturbances inside the bay.

Lastly, the determination of the fuselage low boom configuration uses the most appropriate values according to current studies. The design uses a H/L ratio = 6.0 and y_f/L ratio = 0.04. using these values, the resulting nose width in order to produce a low boom is 2.4 ft. Using these values for the F-function equations for near field pressure signatures should lengthen the overpressure rise times and decrease the effects of the aircraft's sonic boom.

5.6 Conclusion

The developed procedures to minimizing the sonic boom by reshaping the aircraft's fuselage was used to configure the SFAwLT's fuselage design. The design included cockpit design which focused on the pilot ergonomics. Also canopy visibility and drag reduction was implemented in the design. Moreover, the weapons bay design allowed internal storage of all air-to-air missiles. The weapons bay design implemented a cavity shaping design to reduce turbulent and unsteady flows which could had cause shear layers and cabin noise. Lastly, the implementation of the low-boom fuselage configuration provided an unusual bluntness to the aircraft nose. Also, as seen in many low-boom configurations, the nose length was increased. The designed nose length to fuselage ratio (l_f/l_{fn}) was 15. The lengthen nose design was expected to flatten the overpressure peak in the initial shockwave.

6.0 Wing Design

6.1 Wing Design Configuration Selection

The previous Chapter 4.4 discusses the wing configuration selected for this design. This chapter involves the trade studies done for the wing's best performance. Various shapes, dimensions, and angles selections have been determined from the trade study results and iterations of various wing designs. Reasons for the selection of each configuration are also included in the chapter. Table 32 shows the configurations of the wing design.

Table 35 Wing configuration design

Small wing (high W/S)
Cranked arrow delta wing
Low aspect ratio
High wing
Tapered
Swept wing
Anhedral angle
Twisted wing

6.2 Lift Coefficient Requirements

To ensure that the wing design is capable of producing the necessary aerodynamics needed to fly the aircraft, the required lift coefficients must be determined from the selected wing loading. To reiterate from the sizing procedure, the wing loading (W/S) for the aircraft is 110 lbs/ft^2. Equation 6.1 is used to solve the aircraft's cruise lift coefficient. The rest of the required lift coefficients such as for takeoff and landing are the data produced from the RDS performance sizing. Table 33 list the lift coefficients that needs to be met.

$$C_{L,cruise} = W_{TO} - 0.4W_f \, qS \qquad (6.1)$$

Table 36 Lift coefficient requirements for stall speed, takeoff, climb, and landing

$C_{L,max}$	$C_{L,max,TO}$	$C_{L,max,climb}$	$C_{L,max,manuevers}$	$C_{L,cruise}$	$C_{L,max,L}$
1.92	1.191	1.08 – 1.97	1.77	0.13 – 0.64	2.52

6.3 Airfoil selection

Airfoil selection plays a critical role in the aircraft's performance. Not only it is significant in the wing aerodynamics, it also plays a large role in the wings' structure. More importantly, the wings are usually used for fuel storage, thus, wing volume is greatly considered. To ensure that the aircraft is optimal for supersonic speeds, a supercritical airfoil must be used. Supercritical airfoils delay the wave drag production as the wing enters transonic regimes. For this design, a NACA 6 series type of airfoil is used.

Airfoil trade studies were conducted to various NACA 6 series supercritical airfoils. The analysis was conducted using a program called XFLR5, which derives from Xfoil. XFLR5 was able to provide AOA sweeps at various Reynold's numbers. The resulting stall speed from the performance sizing was used to determine the range of Reynold's numbers for the sweep. For the stall speed V_{stall} = 150 mph. the range of Reynold's number was from Re = 6e+6 – Re = 37e+6. The result of the study found that the NACA 64a410 was able to achieve the required $C_{L,max}$ =

1.92. Figure 26 illustrates the geometry of the NACA 64a410 and NACA 64a010 supercritical airfoils. With the outstanding result of the airfoil trade study, the NACA 64a410 airfoil was deemed to be the airfoil used for the wing tips. The same study was conducted for symmetric supercritical airfoil NACA 64a010. The results showed from that sweep that this airfoil was not able achieve the required $C_{l,max}$. However, the NACA 64a010 airfoil was still considered in the design to be used as the wing root airfoil. The intention was so the wing root would stall before the wingtips of the aircraft therefore, maintaining controllability on the ailerons of the wings.
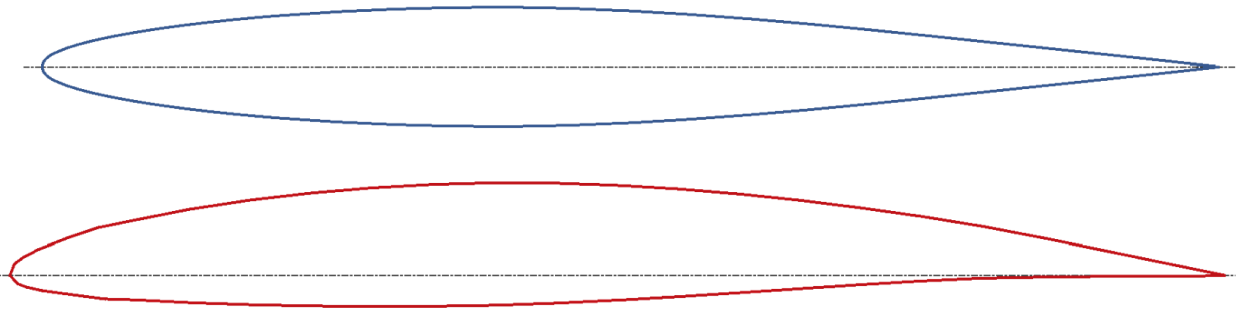
Figure 26 NACA 64a010 with 10% at .4c [top], NACA 64a410 with 10% t/c at .39c and 2.7% camber at .5c [bottom]
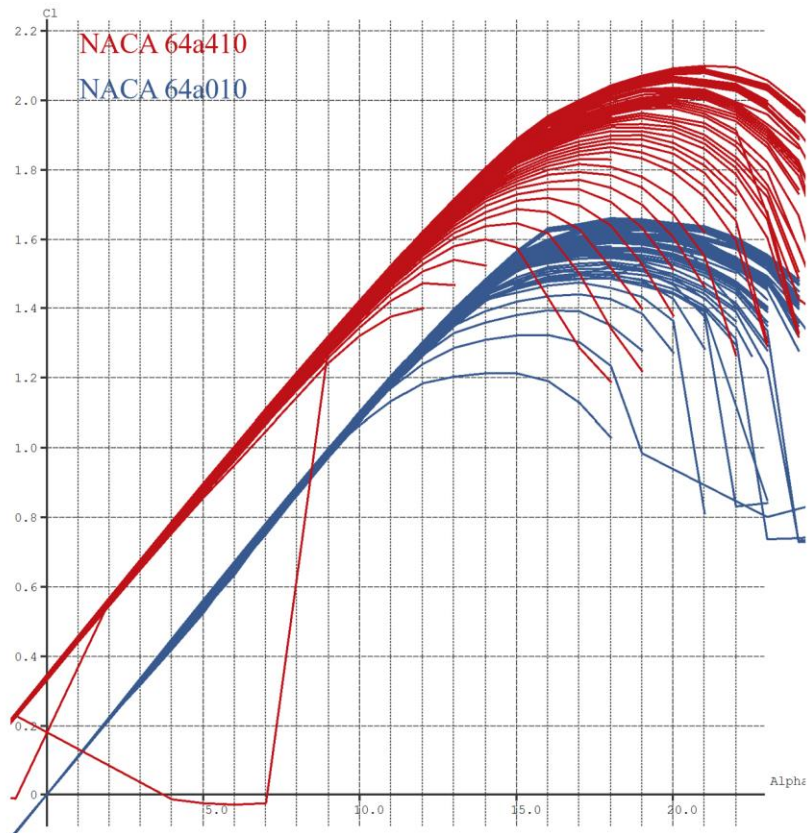
Figure 27 Airfoil AOA sweep at Reynold's numbers Re = 6.0e+6 to Re = 37.0e+6 using XFLR5

6.4   Wing Planform Selection

To determine the proper wing planform for the design, various data from Roskam [27] aircraft design book are used as baseline values. Also, wing planform geometries of the similar aircraft are investigated. More importantly, current wing designs of studied low boom aircraft have also been investigated since these designs have produced positive results. Table 34 contains the wing planform geometries for the low boom design. The surface area in the table is derived from the selected wing loading W/S = 110 lbs/ft^2. Also, the aspect ratio has been predetermined before the wing design according to the similar aircraft data.

Table 37 Wing planform geometry

Parameter	Value
Surface area (S_w)	430.35 ft^2
Aspect ratio (AR_w)	3.0
Wing span (b_w)	36 ft
Taper ratio (λ_w)	0.15
Leading edge sweep ($\Lambda_{w,LE}$)	70°, 60°, 22°
Quarter chord sweep ($\Lambda_{w,c/4}$)	47.5°
Mean geometric chord $\bar{c}_w$	11.95 ft
Mean aerodynamic chord (MAC_w)	17.03 ft
Root chord ($c_{w,root}$)	30 ft
Tip chord ($c_{w,tip}$)	4.575 ft
Dihedral angle (Γ_w)	-1.5°
Wing twist	0

Wing trade study was also conducted once an initial planform was determined. Similarly, the wing study was done using the XFLR5 analysis tool. The type of finite wing analysis used in XFLR5 was the Vortex Lattice Method (VLM). This method was able to provide values for C_L, C_D, C_M and pressure coefficients. However, this method had its short comings such as the unreliability in high angles of attack. Therefore, the Panel method was also used to acquire the same aerodynamic characteristics. Moreover, viscous analysis was added at standard temperature and pressure conditions (STP). Various iterations of wing designs were analyzed using this method to achieve the best maximum lift coefficient $C_{L,max}$. The viscous analyses were not able to provide solutions for every angle-of-attack. The results between $\alpha = 17°$ upto $\alpha = 73°$ were not interpolated by XFLR5, since the airfoil data could not produce the required values for interpolation. Finally, the wing model was designed following the planform in Table 37 was able to achieve such feat. The study focused on the lift performance of the wing. The results show that the designed wing planform was capable of reaching a $C_{L,max} = 2.00$ at a very high AOA = 88°. Note that the resulting $C_{L,max}$ value was determined at the registered stall speed $V_{stall} = 150$ mph. Figure 28 illustrates the various wing designs investigated in the study.

Figure 28 Planform design iterations for wing design analysis

Figure 29 Final wing planform design iteration
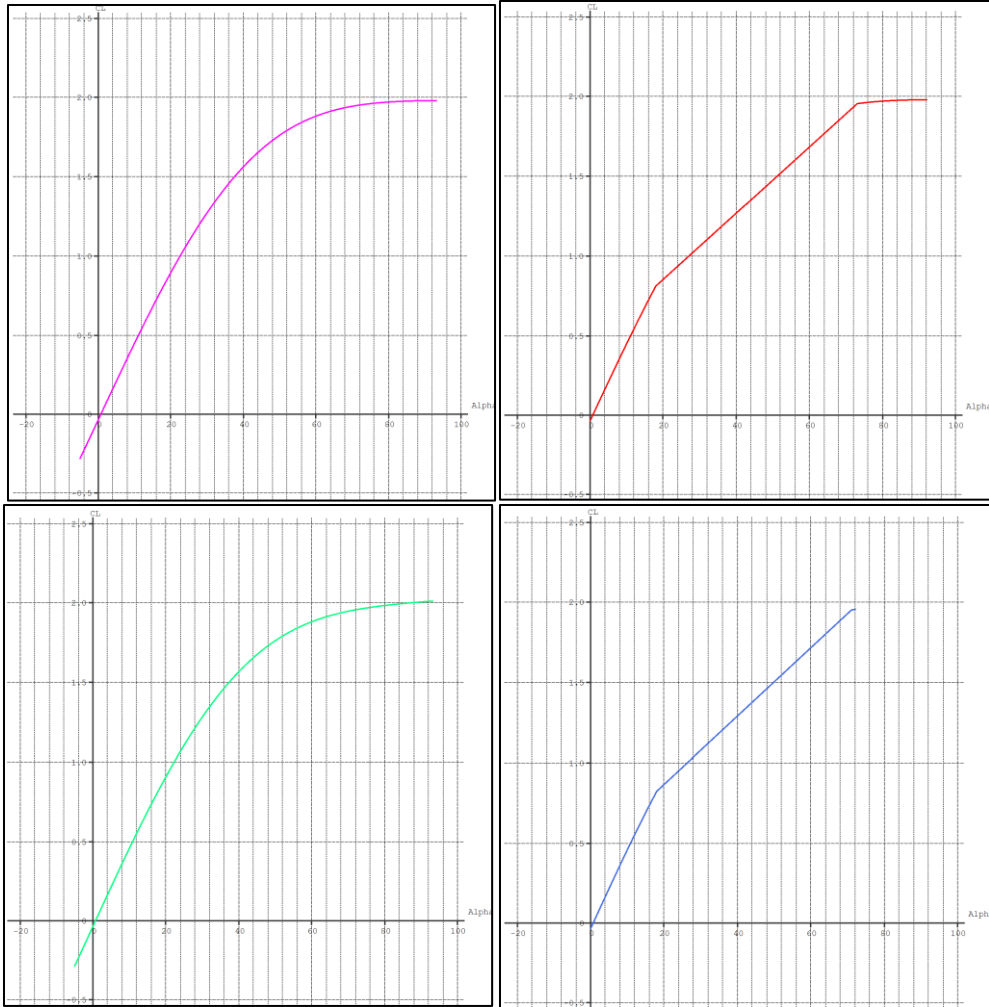
Figure 30 Selected design VLM and Panel method analysis inviscid C_{L},α plot [left] viscous C_{L},α plot [right]
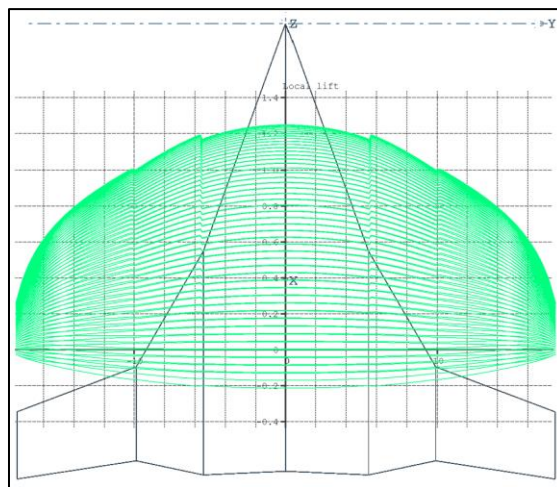
Figure 31 Selected wing planform design local lift distribution executed in XFLR5

The wing planform selection was determined after lengthy trade studies on various planforms. The selected planform performance had the second-best $C_{L,max} = 2.00$. The planform design selected shown in Figure 29 included the geometries such as the root chord (c_{root}) and tip chord (c_{tip}), the leading-edge sweep (λ_{LE}) of the two wing sections, and the entire span of the wing (b). This planform, resembled the cranked-arrow delta wing design from the F-16 XL, discussed in the wing configuration selection above.

6.5 Wing Volume Estimation

Since the wing design an airfoil had been determined, the next step was to calculate the wing's volume for fuel storage. It was intended to integrate a 20% fuel reserve within the wing fuel storage if possible. It was assumed that delta wing configurations were capable to store higher volume of fuel. Roskam's aircraft design part II [27] provided the wing volume for fuel storage. Equation was used to calculate the wing fuel volume. The wing was divided into three sections (main, mid, and tip). Each section's fuel volume was calculated and summed for the total wing fuel volume V_{WF}. Table 35 was added to show the geometries of each section

Table 38 Wing sectional geometries for fuel volume calculation

Section	Surface Area S ft^2	Span b ft	c/4 sweep $\Lambda_{c/4}°$	$(t/c)_{root}$	$(t/c)_{tip}$
Main	247	11	64	.10	.10
Mid	95.85	10	52	.10	.10
Tip	86.65	8	16	.10	.10

$$V_{WF} = 0.54(S^2/b)(t/c)_{root} \left[(1 + \lambda_W \tau_W^{1/2} + \lambda_W^2 \tau_W)/(1 + \lambda_W)^2 \right] \qquad (6.2)$$

$$\text{Where: } \tau_W = (t/c)_{tip} / (t/c)_{root}$$

The result from Equation 6.2 was compared with the required fuel for the entirety of the mission. The fuel capacity of 21,977 lbs was converted into volumetric measurement in cubic feet $V_{fuel} = 352.59$ ft^3. The estimated fuel volume of the wing was $V_{WF} = 388.63$ ft^3. Unfortunately, the wing volume was not capable of storing an intended addition of a 20% fuel reserve volume (70 ft^3). To accommodate the un-stored 10% fuel reserve, an auxiliary fuel volume for the overall 20% fuel reserved was suggested to be stored in tip tanks, slipper tanks, fuselage tanks, or empennage tanks [27]. For this design, additional fuel volume was added in the fuselage tanks aft of the cockpit between the engines.

6.6 High Lift Devices Design

Once the wing planform was determined, next was to design the proper high lift devices to attain the landing maximum lift coefficients $C_{L,max,L}$. As viewed in table 36, a $C_{L,max,L} = 2.52$ was required for achieving the required landing field length. Since the clean $C_{L,max} = 2.003$, the takeoff maximum lift coefficient $C_{L,max,TO}$, did not require a high lifting device configuration. In order properly design the required high lifting device to achieve the $C_{L,max,L} = 2.52$, the $C_{l,max,L}$ was calculated using Equation 6.3. The resuling $c_{l,max,L}$ was then used to calculate -- as seen in Equation 6.5 -- the required incremental lift coefficient $\Delta c_{l,L}$ the flap must be able to provide.

$$\Delta c_{l,max,L} = (\Delta C_{L,max,L})(S/S_{wf}) / (K_\Lambda) \qquad (6.3)$$
$$\text{where: } S/S_{wf} \text{ is the flap to wing area ratio}$$

$$K_\Lambda = (1 - 0.08\cos^2(\Lambda_{c/4}))\cos^{3/4}(\Lambda_{c/4}) \tag{6.4}$$

where: K_Λ accounted for the wing sweep
angle effect during flaps down configuration

$$\Delta c_l = (1/K)\,\Delta c_{l,max,L} \tag{6.5}$$

where: the factor K can be found in Figure 6.7
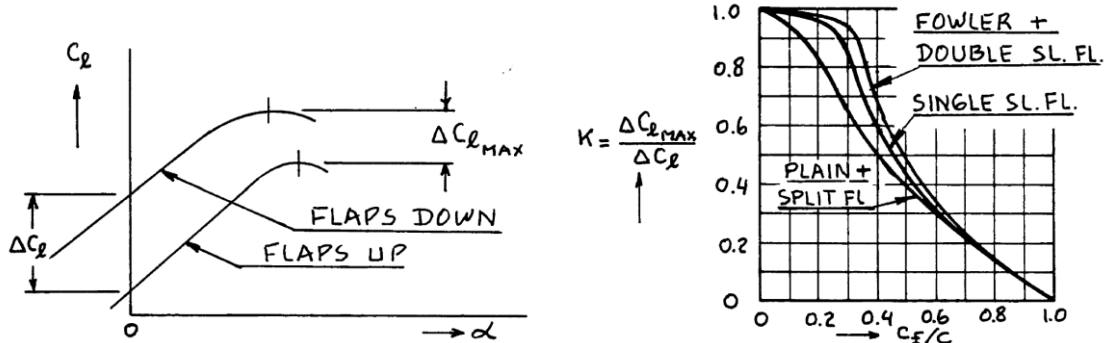
Figure 32 $\Delta c_{l,max,L}$ and Δc_l relation and factor K ratio for calculating Δc_l
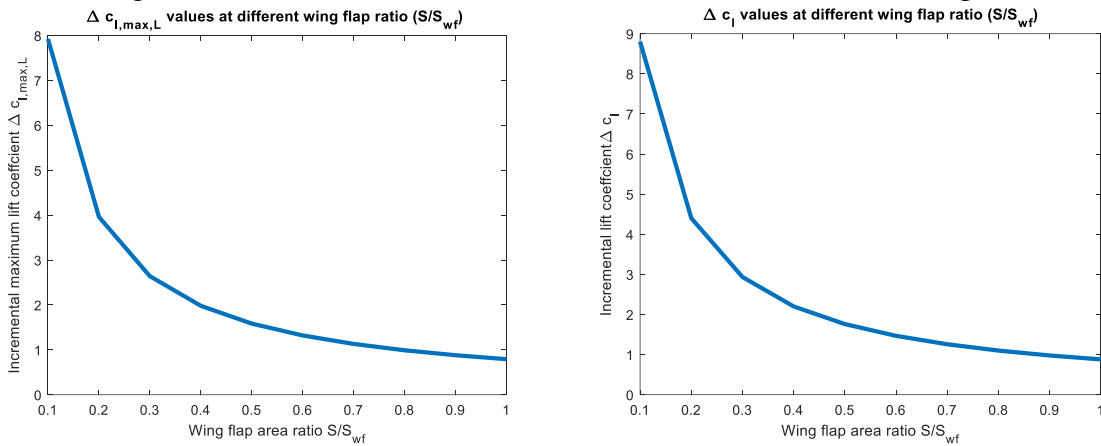
Figure 33 $\Delta c_{l,max,L}$ and Δc_l values according to various S_{wf}/S
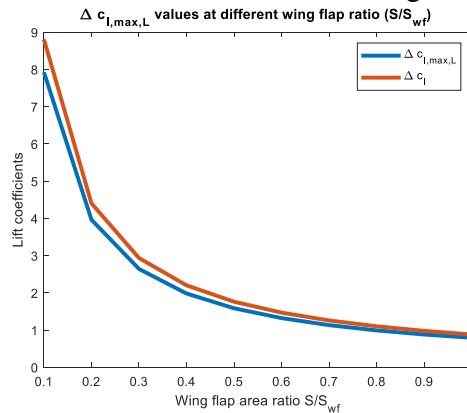
Figure 34 Actual calculated and $\Delta c_l = 1.65$ values with $\Delta c_{l,max,L} = 1.32$ and K = 0.9

To achieve the resulting incremental lift coefficient, a flaperon configuration was integrated on the wing. The flaperon was a plain flap at the trailing edge of the wing located adjacent to the aileron. Additionally, a combination of a split flap and a slat was investigated to

help increase both the $C_{L,max,L}$ and the stall maximum angle-of-attack. The initial step was to determine the trailing edge flap combination. As seen in Figure 33, a flap chord ratio $c_f/c = 0.2$ satisfied the 0.8 K factor that was used in Equation 36 to achieve the best Δc_l possible. The calculated the maximum lift coefficient produced by the plain flaperon, split flap and slat Equation 6.6, Equation 6.7, and Equation 6.8 were used.

$$\text{Plain flaps: } \Delta c_l = c_{l,\delta_f} \, \delta_f K' \tag{6.6}$$

where: δ_f to K' relationship is shown in Figure 6.9

$$\text{Split flaps: } \Delta c_l = k_f(\Delta c_{l,c_f/c=0.2}) \tag{6.7}$$

where: c_f/c to k_f relationship is shown in Figure 6.10

$$\text{Slats: } c_{l,max \text{ with LE flap}} = c_{l,max \text{ no LE flap}} (c''/c) \tag{6.8}$$

where: c''/c is defined in Figure 6.11
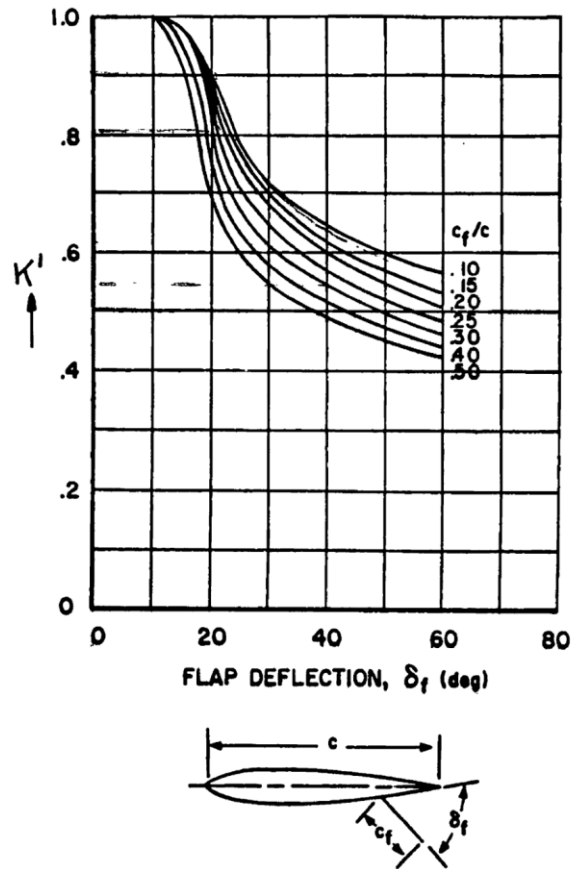
Figure 35 Effect of chord ratio to flap deflection
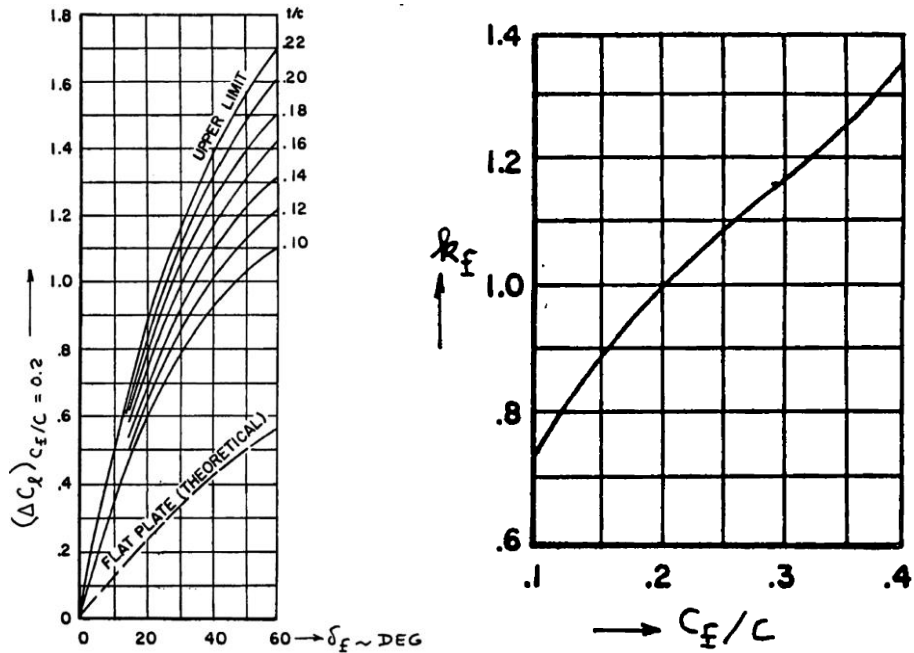
Figure 36 Split flap Δc_l calculation empirical data
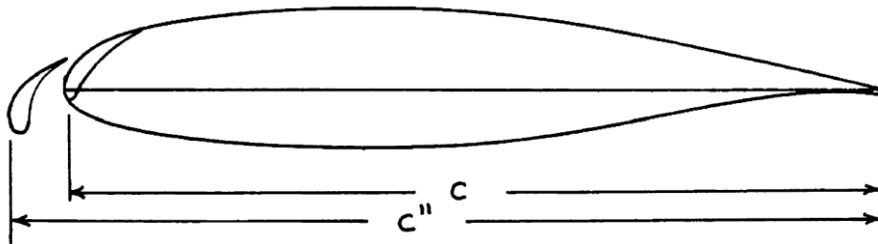
Figure 37 Leading edge slat definition of c''/c

Table 39 High lift devices integration data

High lift device	S_{wf}/S	b_f/b	c_f/c	c''/c	δ_f	Δc_l	$\Delta c_{l,max,L}$	$C_{L,max,L}$
No flap	--	--	--	--	--	--	--	2.00
Plain flaperon	0.1	0.22	0.3	--	40°	0.74	0.59	2.10
Split flap	0.2	0.25	0.2	--	40°	1.3	1.17	2.33
LE slat wing (mid)	0.2	0.25	--	1.1	--	--	0.15	2.47
LE slat wing (tip)	0.2	0.44	--	1.1	--	--	0.2	2.62
Combination	--	--	--	--	--	--	--	3.52
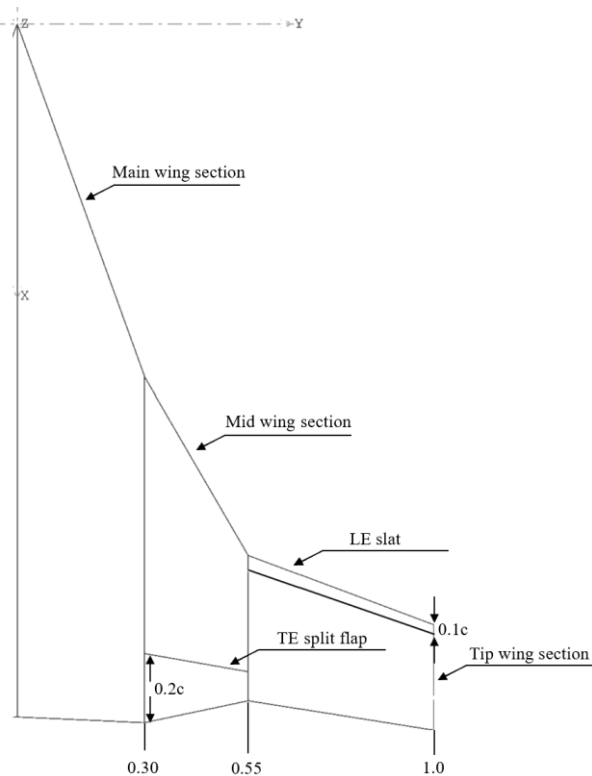
Figure 38 Wing high lift devices type, location and geometry

6.7   Vertical Stabilizer and Control Surfaces Design

The empennage configuration discussed in Chapter 4 only include a vertical stabilizer. Lowering the empennage area was considered to be greatly beneficial to the aircraft's weight and improve its stealth characteristics. Achieving this design required a high vertical stabilizer moment arm x_v relative to the critical center of gravity c.g (most aft c.g. location). To determine the proper stabilizer design, pervious aircraft data of similar parameters in Table 37 were investigated.

Table 40 Fighter aircraft empennage and control surfaces data [stabilator *]

Type	Hor. stab area S_h ft^2	Vert. stab area S_v ft^2	S_r/S_v	S_e/S_h	x_h ft	x_v ft	$\bar{V}_h$	$\bar{V}_v$	Rudder chord root/tip fr.c_v	Elevator chord root/tip fr.c_h	S_a/S	Aileron span loc. in/out fr.b/2	Aileron chord in/out fr.c_w
F-14A	140	118	.29	1.0	16.4	18.4	.40	.06	.29/.33	*	--	--	--
F-15	104	143	.25	1.0	20.7	17.8	.20	.09	.30/.50	*	.053	.60/.86	.25/.27
SFAwLT	30	58	.23	--	17	16	.10	.06	.38/.25	.09/.18	.062	.64/1.0	.27/.32

The empennage designs seemed the best baseline parameter to be considered for this aircraft's vertical stabilizer's design. The strategy was to select a minimum and maximum baseline moment arm x_v and vertical stabilizer volume coefficient $\bar{V}_v$. Various iteration for the best S_v was calculated using Equation 6.9.

$$S_v = \bar{V}_v S b / x_v \qquad (6.9)$$

The vertical planform followed the suggested design parameters from Roskam [27]. Much like the wing design process, the selected vertical tail area S_v was the initial design parameter, where the other parameters must keep the same.

Now that the wing, high lift devices and vertical stabilizer were designed, the last important part of the wing design were the control surfaces. The control surfaces included the rudder for yaw, elevators for pitch and ailerons for roll. Since the empennage design did not include a horizontal stabilizer, the design for the elevator surface was performed differently. Fighter aircraft elevator surface area ratio $S_e/S_v = 1.00$. Therefore, the design surface area was compared to aircraft data horizontal tail surface area S_h. To calculate the desired S_h value to use for the elevator area ratio, Equation 6.10 was used. Once the horizontal stabilizer surface area S_h was calculate, the elevator surface area S_e was equated.

$$S_h = \bar{V}_h S \bar{c} / x_h \qquad (6.10)$$

Lastly, the aileron design used aircraft data with similar wing surface area and wing span for comparison. Data from Roskam [27]. Noted that the aileron span had a limit according to wing section it was integrated into (wing tip section). The aileron design comparable to the data provided resulted in aileron span $b_A = 0.44(b/2)_w$ and aileron chord c_A locations $= 0.27c_w/0.32c_w$ (in/out) with a the aileron surface area ratio $S_a/S = 0.062$. Additionally, the vertical stabilizer rudder surface control design must be compatible with the aileron design due to the coupling effects of the two control surfaces. The aileron surface area ratio $S_a/S = 0.062$, where it equated to a rudder surface area ratio $S_r/S_v = 0.23$. The calculated rudder chord c_r locations resulted with a rudder span $b_r = b_r/b = 0.8125$. Therefore, the final rudder design's chord locations were placed at $c_{r,root} = .38c_v$ and $c_{r,tip} = .25c_v$.

6.8   Discussion

The wing planform design took various iterations in order to achieve the necessary $C_{L,max}$ value. The last design achieved the requirement, and was verified by the XFLR5 airfoil analysis tool. The planform resembles the F-16 XL cranked-arrow delta wing. It was difficult to achieve such a high $C_{L,max}$ because of the low surface area, span. Also, the wing sweep was design to be a high as possible which was achieved to disrupt the wave drag during supersonic flight. Lastly, the wing planform fuel volume was large enough to store the fuel for the entire mission; however, the 20% fuel reserve were not able to be stored. The 20% fuel reserve if needed, can be stored in the fuselage.

After performing the calculation for each high lift devices, the required $C_{L,max,L} = 2.52$ was determined achievable. The total maximum lift produced by the combinations of high lift devices was outstanding. It was decided that the achieved maximum lift coefficient was too high, therefore, only a select few of high lift devices were chosen. The integrated high lift devices were a combination of trailing edge split flap and the leading-edge slat on the wing tip section. In total, the achieved maximum lift coefficient for landing with the use of high lift devices was $C_{l,max,L} = 2.95$.

To complete the aircraft wing design, control surfaces were designed to achieve the praised fighter aircraft maneuverability and controllability. The empennage designed included a vertical stabilizer but did not cover a horizontal stabilizer since the aircraft configuration was a

delta wing. It was discussed that the vertical stabilizer size and weight must be at a minimum. Therefore, the moment arm for the vertical stabilizer x_v selected was the maximum allowable length to which produced a minimum vertical stabilizer surface area S_v. More importantly, the control surfaces designed did not include any complex combinations such as elevons, flaperon, or spoilers which was investigated during the trade study. The resulting control surface designs were highly comparable to the similar aircraft data for the F-14 and F-15 fighter aircraft.

Finally, the entire wing planform design proved to be workable for the design requirements. There were many iterations and trade study done to achieve the target planform. Figure 39 illustrates the complete and final wing planform which includes the wings, high lift devices and control surfaces.
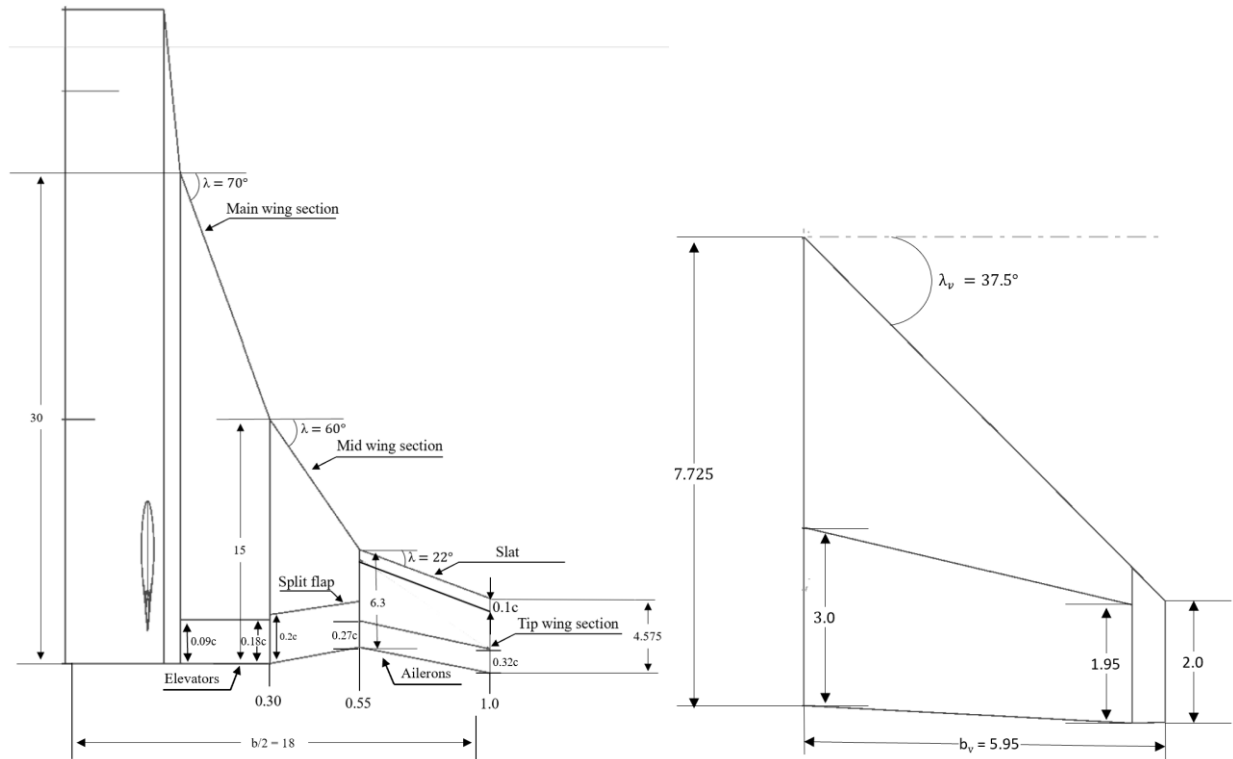
Figure 39 Final wing planform with high lift devices and control surfaces [left] vertical stabilizer with rudder design [right]

6.9 Conclusion

In all, the wing design was a combination of considerations between fighter aircraft capabilities and low boom performance. The design had gone exactly as to how it was first envisioned. However, more analysis could have been included to ensure the aerodynamics of the aircraft. The wings, high lift devices, and control surfaces must be analyzed for the stability and controllability in future time.

7.0 Propulsion System

7.1   Propulsion System Selection

Next step into the design was to select the proper propulsion system to achieve the required mission performance. The required thrust-to-weight ratio T/W was sized in the early chapters. The selected T/W = 1.3 accounted to a thrust availability of 61,384 lbs with afterburner. To achieve this large force requirement, the design must cover number, type of, and performance of the engines.

7.2   Engine Selection
7.2.1   Number of Engines

Proper research of various jet engines was done to ensure that the required available thrust was met. The number of engines used play significant roles in the aircraft's performance. One of the most important studies done for engine selection was the probability of engine failure. Table 41 provided engine probability failure for various numbers of engines used. The best possible choice selected for the aircraft was a two-engine configuration, which was enough to lower the probability of losing both engines to failure.

Table 41 Engine failure probability according to number of engines [27]

Failure of:	1 Engine	2 Engines	3 Engines
Airplane with:			
two engines	$2P_{ef}$	P_{ef}^2	not appl.
three engines	$3P_{ef}$	$3P_{ef}^2$	P_{ef}^3
four engines	$4P_{ef}$	$6P_{ef}^2$	$4P_{ef}^3$

With two engines, next was to select the proper type of engines. The most common engines for fighters were turbofan and turbojet engines. Turbofan engines were known to have a high or low bypass ratio in contrast to a turbojet engine which were purely jet streams with no bypass flow around the jet engine. Data and research favored the use of a turbofan jet engine, more specifically, low bypass ratio turbofan jet engines. Low bypass turbofan engines efficiency at high speeds are reported to be the best of the two engines. Furthermore, additional thrust maybe be available with an afterburner integrated in the engine. Similar aircraft engines were compared to figure out which engine was best for the SFAwLT propulsion system. Figure 40 shown below illustrates the selected power plant that provide the necessary required thrust. Moreover, Table 42 provided contains the performance and characteristics of the selected power plant.

Table 42 Pratt & Whitney F100-PW-229 turbofan engines with afterburners characteristics and performance

Thrust dry	Thrust afterburner	Weight	Length	Inlet diameter	Maximum diameter	Bypass ratio	Overall pressure ratio
lbs	lbs	lbs	in	in	in		
17,900	29,160	3,826	191	34.8	46.5	0.36	32:1
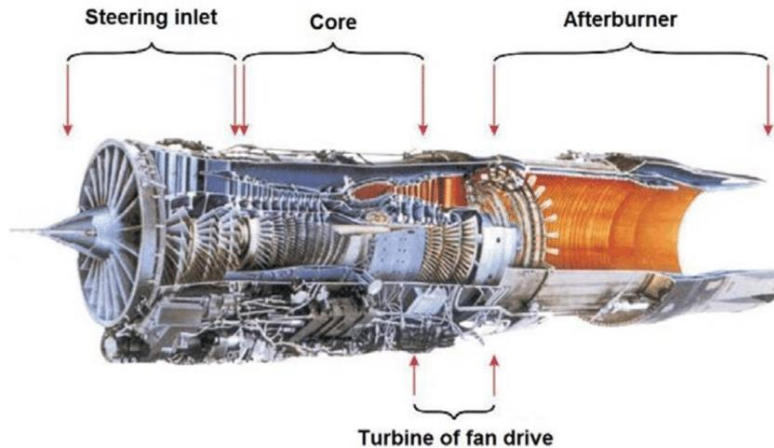
Figure 40 Pratt & Whitney F100-PW-229 turbofan engines with afterburners

7.3   Air Intake Design

Air intake ducts play significant roles in the aircraft's power output. The airflow is strategically designed to benefit the engines power production. The air intake design uses an inward streamline-traced external-compression (STEX) inlet. Results from studies show significant decrease in wave drag and slight decrease in overpressure signatures of the intake. Compared to other inlet designs such as an asymmetric spike and two-dimensional inlets, the STEX delivers a magnitude lower in wave drag, and about a hundredth lower in pressure recovery [34]. Figure 41 shows the basic layout of an inward-turning STEX inlet of an engine intake system. Using this design is greatly beneficial for the low-boom requirement as well as significantly lowering the wave drag during supercruise segments.
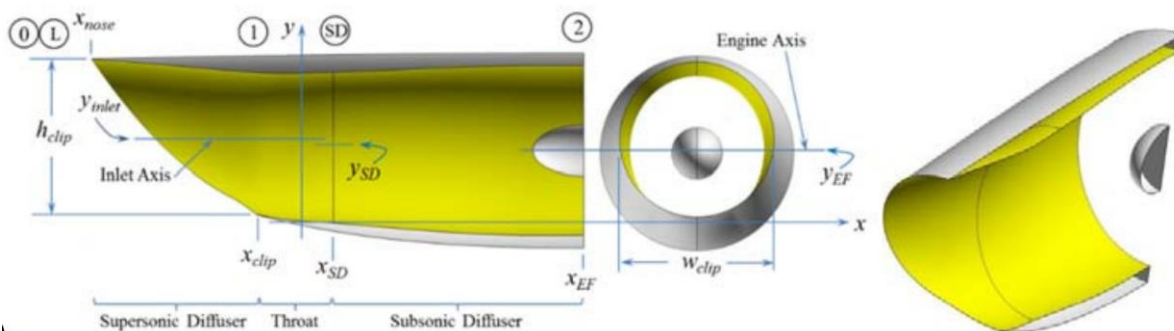
Figure 41 Inward-turning STEX inlet design layout

7.4   Discussion and Conclusion
    The powerplant selection considered various engines commonly used for fighter aircraft. With two engines, a total of 58,000 lbs was considered to be the available thrust. The P&W F100-PW-229 engine used for the F-15 fighter aircraft managed to produce 95% of the required available thrust. To be able to achieve the T/W = 1.3, the design required all possible way to reduce the aircraft weight. More importantly the engine's dimensions allowed internal installation with in the fuselage. In addition, an inlet design was studied for sonic boom reduction. The inward-turning STEX air intake showed results in lowering over pressures, thus can lower the sonic boom. Integration of this propulsion system concept needed verification and additional analysis to verify the thrust availability and low boom characteristics of the air intake.

8.0   Final Design Conclusion
At this point, the design covered the sizing, configurations, and design of the aircraft. The current design seemed to produce acceptable results for a fighter aircraft. More importantly, various aspects of the low boom technology were integrated properly in the:

- Fuselage design
- Air intake design
- Wing design

The fuselage was design for a single pilot cockpit. Also, internal weapons bay was integrated in the desing to ensure minimum drag characteristics at subsonic and supersonic flight. Lastly, the fuselage layout incorporated a blunt nose low boom technique, and low wave drag geometries. The propulsion design used an inward turning STEX inlet where studies showed to minimize the sonic boom produced by the air intake, this also provided better flow for the engines for maximum performance.

More importantly, the wing planform resembled the F-16 XL experimental aircraft. The wing geometry was able to achieve low induced drag properties, while also achieving the necessary maximum lift coefficients with the use of high lift devices. The final design of the aircraft are portrayed in a 3-view sketch in Figure 42.

For future considerations, much work is need to verify the full performance of the aircraft. Next steps include:

- Conducting proper weight and balance
- Landing gear design
- Stability and controllability of the aircraft design
- Overall drag polar
- Computational Fluid Analysis of shockwave overpressure and underpressures
- Verify CFD analysis results with low boom data

Side view

Top view

Front view
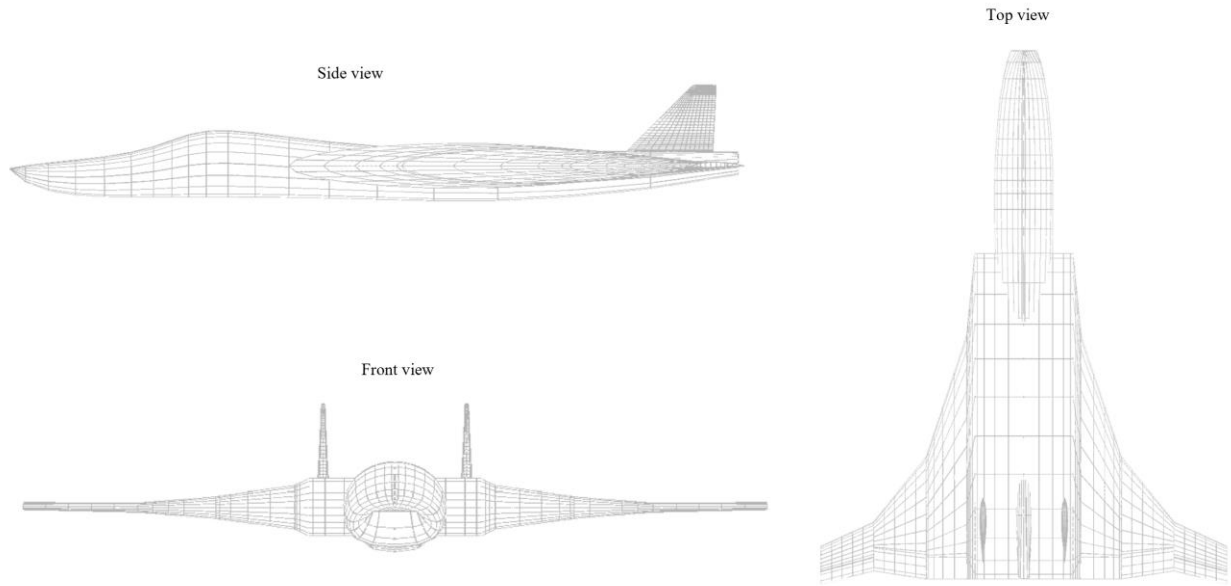
Figure 42 SFAwLT 3-view sketch without the propulsion system

References

[1]   Varnier, J., Le Pape, M.-C., and Sourgen, F., "Ballistic wave from projectiles and vehicles of simple geometry," AIAA Journal, vol. 56, pp. 2725–2742, Jul. 2018 http://dx.doi.org/10.2514/1.J056239

[2]   R. Seebass and A. R. George, "Sonic-Boom Minimization", The Journal of the Acoustical Society of America 51, 686-694 1972 https://doi.org/10.1121/1.1912902

[3]   Ban, N., Yamazaki, W., and Kusunose, K., "Low-boom/low-drag design optimization of innovative supersonic transport configuration," Journal of Aircraft, vol. 55, pp. 1071–1081 2018 https://doi.org/10.2514/1.C034171

[4]   Kamal, A. M., and Ramirez-Serrano, A., "Systematic methodology for aircraft concept development with application to transitional aircraft," Journal of Aircraft, vol. 57, pp. 179–197, 2020 https://doi.org/10.2514/1.C035437

[5]   Li, W., and Geiselhart, K., "Multidisciplinary design optimization of low-boom supersonic aircraft with mission constraints," AIAA Journal 2021, vol. 59, 2020 https://doi.org/10.2514/1.J059237

[6]   Darden, C. M., Sonic-Boom Minimization with Nose-Bluntness Relaxation Hampton, Virginia: NASA Langley, 1979.

[7]   Chiba, K., Makino, Y., and Takatoya, T., "Design-Informatics Approach for intimate configuration of Silent Supersonic Technology Demonstrator," Journal of Aircraft, vol. 49, pp. 1200–1211, Oct. 2012 http://dx.doi.org/10.2514/1.C031116

[8]   Smolka, J. W., Cowert, R. A., and Molzahn, L. M., "51st SETP Symposium," Flight Testing of the Gulfstream Quiet SpikeTM on a NASA F-15B, 2007

[9]   Feng, X., Li, Z., and Song, B., "Research of low boom and low drag supersonic aircraft design," Chinese Journal of Aeronautics, vol. 27, pp. 531–541, 2014 http://dx.doi.org/10.1016/j.cja.2014.04.004

[10]   Greenblatt, D., Whalen, E. A., and Wygnanski, I. J., "Introduction to the flow control virtual collection," AIAA Journal, vol. 57, pp. 3111–3114, Aug. 2019 http://dx.doi.org/10.2514/1.J058507

[11]   Warsop, C., and Crowther, W. J., "Fluidic flow control effectors for flight control," AIAA Journal, vol. 56, pp. 3808–3824, Oct. 2018 http://dx.doi.org/10.2514/1.J056787

[12]   Kanamori, M., Ishikawa, H., Naka, Y., and Makino, Y., "Numerical simulation of diffracted U-shaped Sonic boom waveform," AIAA Journal, vol. 60, pp. 2787–2797, May 2022 https://doi.org/10.2514/1.J060477

[13]   Kanamori, M., Takahashi, T., Ishikawa, H., Makino, Y., Naka, Y., and Takahashi, H., "Numerical evaluation of sonic boom deformation due to atmospheric turbulence," AIAA Journal, vol. 59, pp. 972–986, Mar. 2021 https://doi.org/10.2514/1.J059470

[14]   Lengyan, and Zhansen, Q., "A CFD based Sonic Boom Prediction Method and investigation on the parameters affecting the Sonic Boom Signature," Procedia Engineering, vol. 99, pp. 433–451, 2015 https://doi.org/10.1016/j.proeng.2014.12.558

[15]   Li, W., and Geiselhart, K., "Integration of low-fidelity MDO and CFD-based redesign of low-boom supersonic transports," AIAA Journal, vol. 59, pp. 3923–3936, Oct. 2021 https://doi.org/10.2514/1.J060368

[16]   Yamashita, R., Makino, Y., and Roe, P. L., "Fast full-field simulation of Sonic Boom using a space   marching method," AIAA Journal, vol. 60, pp. 4103–4112, 2022 https://doi.org/10.2514/1.J061363

[17] "*Mikoyan MiG-31 (FOXHOUND)* Available: https://www.militaryfactory.com/aircraft/detail.php?aircraft_id=65, retrieved June 2022

[18] Palt, K., *Grumman F-14 Tomcat - specifications - technical data / description* Available: http://www.flugzeuginfo.net/acdata_php/acdata_f14_en.php, retrieved June 2022

[19] "1 introduction," *Designations Of U.S. Military Aero Engines.* Available: http://www.designation-systems.net/usmilav/engines.html#_MILSTD1812_AirBreathing , retrieved June 2022

[20] Gunston, B., *World encyclopaedia of aero engines*, Stephens, 1989.

[21] Air Force History, and Neufeld, J., Office of Air Force History, 1974.

[22] Gordon, Y., *Flight craft 5: Sukhoi su-15 - the boeing killer*, Pen & Sword Books Ltd, 2015.

[23] Neufeld, J., *The F-15 Eagle, origins and development, 1964-1972*, Office of Airforce History, 1974.

[24] Roskam, J., *Airplane design I: Preliminary sizing of airplanes*, Lawrence, KS: DAR Corporation, 1997.

[25] Raymer, D. P., *Aircraft design: A conceptual approach*, American Institute of Aeronautics and Astronautics, 2018.

[26] Yang, Y., and Zha, G., "Super-lift coefficient of active flow control airfoil: What is the limit?," 55th AIAA Aerospace Sciences Meeting, 2017.

[27] Roskam, J., *Airplane Design II: Preliminary Configuration Design and Integration of the Propulsion System*, Lawrence, KS: DARcorporation, 1997.

[28] Benson, L. R., *Quieting the Boom: The Shaped Sonic Boom Demonstrator and the Quest for Quiet Supersonic Flight*, Washington, D.C.: National Aeronautics and Space Administration, 2013.

[29] Roskam, J., *Airplane Design III: Layout Design of Cockpit, Fuselage, Wing and Empennage: Cutaways and Inboard Profiles*, Lawrence, KS: DAR Corporation, 2002.

[30] Makino, Y., Sugiura, T., Watanuki, T., Kubota, H., Aoyama, T., Iwamiya, T., Makino, Y., Sugiura, T., Watanuki, T., Kubota, H., Aoyama, T., and Iwamiya, T., "The effect of nose bluntness of a low-boom configuration on Sonic-Boom," *15th Applied Aerodynamics Conference*, 1997.

[31] Dunbar, B., "F-16XL ship #2 Supersonic laminar flow control," *NASA* Available: https://www.nasa.gov/centers/dryden/history/pastprojects/F16XL2/index.html. retrieved October 20, 2022

[32] Roskam, J., *Airplane Design IV: Layout Design Of Landing Gears And Systems*, Lawrence, KS: DAR Corporation, 1989.

[33] Bacci, D., Design of Weapon Bays for Stealth Aircrafts, 2017.

[34] Otto, S. E., Trefny, C. J., and Slater, J. W., "Inward-turning streamline-traced inlet design method for low-boom, low-drag applications," *Journal of Propulsion and Power*, vol. 32, pp. 1178–1189, 2016. https://doi.org/10.2514/1.B36028